Anomalous Spectral Lines in Space and Laboratory Plasmas - Studies with HST and CRYRING

Hartman, Henrik

2003

Anomalous spectral lines in space and laboratory plasmas

Studies with HST and CRYRING

Henrik Hartman

Atomic Astrophysics
Lund Observatory
Lund University
Sweden

Thesis for degree of Doctor of Philosophy

Thesis advisor: Prof. Sveneric Johansson

To be presented, with the permission of the Faculty of Science of Lund University, for public criticism in the Lundmark lecture hall (Lundmarksalen) of Lund Observatory on Friday, the 19th of December, at 10.15 a.m.

Organization **LUND UNIVERSITY** Lund Observatory Box 43 SE-221 00 Lund, Sweden	**Document Name** **DOCTORAL DISSERTATION** **Date of issue** 19 Dec, 2003 **CODEN:**
Author(s) Henrik Hartman	**Sponsoring organization**
Title and subtitle Anomalous spectral lines in space and laboratory plasmas Studies with HST and CRYRING	

Abstract

Eta Carinae is one of the most massive and luminous stars in the Galaxy. A huge bipolar nebula and an equatorial disk give the object a characteristic shape. Close to the star there are gas clouds, which emit intriguing emission line spectra. One such region, the strontium filament, is studied in more detail in this thesis, and the identities of 600 emission lines are reported. Some of these require extra treatment, viz. allowed and forbidden lines of Ti II and Sr II.

Many thin astrophysical plasmas emit parity-forbidden lines, which can be used to diagnose the plasma. The upper levels of these lines are metastable states, which have radiative lifetimes of the order of 1 second compared to 1 nanosecond for ordinary states. We have performed measurements of metastable lifetimes in complex ions applying a laser probing technique on a stored ion beam at the storage ring CRYRING (MSL, Stockholm). This thesis reports on 4 lifetimes in Fe II and 2 in Ti II, the first measured in such complex systems. The lifetimes are in the range 0.23 to 28 s.

Experimental absolute transition probabilities for forbidden lines in [Fe II] are derived by combining the experimental metastable lifetimes with astrophysical branching fractions (BF). The BF's are derived from spectra of the Weigelt blobs of Eta Carinae, which contain strong forbidden [Fe II] lines.

In some stars the intensity of emission lines from specific high-excitation levels is greatly enhanced. They are explained as fluoresence lines from energy levels, which have an enhanced population due to selective photoexcitation. This is caused by an accidental coincidence in wavelength between a strong emission line and the pumped transition. We report on fluorescence lines and pumped levels in Fe II observed in the symbiotic star RR Telescopii.

Key words Atomic Spectroscopy, lifetime measurements, line identification, fluorescence, forbidden lines, metastable levels, RR Telesopii, Eta Carinae, HST, STIS, CRYRING, iron, titanium, strontium

Classification system and/or index terms (if any)

Supplementary bibliographical information
LUNFD6/(NFAS 1027)/1-176/(2003)

Language English

ISSN and key title

ISBN
91-628-5903-X

Recipient's notes

Number of pages 176

Price

Security classification

Distribution by (name and address)
Henrik Hartman, Lund Observatory, Box 43, SE-221 00 Lund, Sweden
henrik.hartman@astro.lu.se

November, 2003

Signature _____ **Date** _____

Vetenskapsmannen studerar inte naturen därför att det kan vara till nytta. Han studerar den därför att han finner nöje i den och han finner nöje i den därför att den är vacker.

Henri Poincaré, 1908

This thesis is based on the following publications:

I **Ultraviolet fluorescence lines of Fe II observed in satellite spectra of the symbiotic star RR Telescopii**
Hartman, H., Johansson, S.
A&A **359**, 627 (2000)

II **New forbidden and fluorescent Fe III lines identified in HST spectra of η Carinae**
Johansson, S., Zethson, T., **Hartman, H.**, Ekberg, J.O., Ishibashi, K., Davidson, K., Gull, T.
A&A **361**, 977 (2000)

III **Sr II and [Sr II] Emission in the Ejecta of Eta Carinae**
Zethson, T., Gull, T., **Hartman H.**, Johansson, S., Davidson, K., Ishibashi, K.
AJ **122**, 322 (2001)

IV **Excitation of Sr II lines in Eta Carinae**
Bautista, M. A., Gull, T.R., Ishibashi, K., **Hartman H.**, Davidson, K.
MNRAS **331**, 875 (2002)

V **Identification of Emission Lines in the Low-Ionization Strontium Filament Near Eta Carinae**
Hartman, H., Gull, T.R., Johansson, S., Smith, N., HST Eta Carinae Treasury Project Team
Submitted to A&A

VI **Lifetime Measurements of Metastable States in Fe^+**
Rostohar, D., Derkatch, A., **Hartman, H.**, Johansson, S., Lundberg, H., Mannervik, S., Norlin, L.-O., Royen, P., Schmitt, A.
Phys. Rev. Lett. **86**, 1466 (2001)

VII **The FERRUM Project: Experimental transition probabilities of [Fe II] and astrophysical applications**
Hartman, H., Derkatch, A., Donnelly, M. P., Gull, T., Hibbert,A. , Johansson, S., Lundberg, H., Mannervik, H., Norlin, L.-O., Rostohar, D., Royen, P., Schef, P.
A&A **397**, 1143 (2003)

VIII **The FERRUM project: an extremely long radiative lifetime in Ti II measured in an ion storage ring**
Hartman, H., Rostohar, D., Derkatch, A., Lundin, P., Schef, P., Johansson, S., Lundberg, H., Mannervik, S., Norlin, L.-O., Royen, P.
J. Phys. B Letter **36**, L197 (2003)

Related work, not included in thesis:

The FERRUM project: New f-value Data for Fe II and Astrophysical Applications
Johansson, S., Derkatch, A., Donnelly, M.P., **Hartman, H.**, Hibbert, A., Karlsson, H., Kock, M., Li, Z.S., Leckrone, D.S., Litzén, U., Lundberg, H., Mannervik, S., Norlin, L.-O., Nilsson, H., Pickering, J., Raassen, T.,Rostohar, D., Royen, P., Schmitt, A., Johanning, M., Sikström, C.M., Smith, P.L., Svanberg, S., Wahlgren, G.M.
Physica Scripta **T100**, 71 (2002)

Experimental investigation of radiative decay rates of metastable levels in Eu II
Rostohar, D., Andersson, K., Derkatch, A., **Hartman, H.**, Mannervik, S., Norlin, L.-O., Royen, P., Schmitt, A., Tordoir, X.
Physica Scripta **64**, 237 (2001)

My contribution to each paper is specified explicitly in Section 6 in connection with the presentation of the papers.

The cover shows an ACS/HRC picture of Eta Carinae (Smith et al. 2004), and a HST/STIS spectrum of the strontium filament with e.g. forbidden lines of [Sr II] and [Ti II] (Paper V). A lifetime curve from the measurements of $b^4P_{5/2}$ in Ti II (Paper VIII) is shown in the upper right corner.

Contents

x

Chapter 1

Introduction

The majority of the chemical elements building up ourselves and our world are, except for the lightest ones, produced in stars. Depending on the inherent properties of the star different elements are created. During its life, and especially during the late phases, the star returns material to the surrounding medium from which it was once formed. The evolution of stars is thus important in the understanding of the chemical evolution of the Galaxy.

Massive stars live, on a relative scale, a fast and hectic life ending with a grand finale when they return their chemical contents to the environment in a supernova explosion. Some heavy elements are even believed to be produced in these large explosions. One of the most massive and spectacular stars in our Galaxy is Eta Carinae with a mass of more than 130 $M_{\odot}$ and 5 million times more luminous than the sun[1]. The star has experienced the most energetic non-terminal outburst known, i.e. expelling large amounts of mass and energy without collapsing. During a 7-8 year period around 1840 it brightened from about 3^{rd} to -1^{st} magnitude and became the second brightest star in the sky, although being 7500 light years away[2]. A result of this 'Great Eruption' is today observed as a beautiful bipolar structure, called *the Homunculus*. Its lobes contain a few solar masses of material and move outwards with a speed of several hundreds km/s.

Eta Carinae has been intensively studied since the first spectrum was taken in 1893. The basic spectroscopy in the optical region has been complemented by ultraviolet and infrared observations using space-borne and ground-based instruments. The Hubble Space Telescope (HST) and its Space Telescope Imaging Spectrograph (STIS) have opened the possibility to combine a good spectral resolution with a spatial resolution that can re-

[1] Humphreys et al. (2002); Davidson & Humphreys (1997)
[2] Humphreys & Davidson (1994)

solve different parts of the nebula[3]. Despite large analysis efforts some key properties of the star are poorly understood, e.g. what initiated the Great eruption. Neither is the nature of the central object, a single or binary star, nor the periodic spectroscopic events described below understood.

On a smaller timescale, Eta has experienced what is called *spectroscopic events* with a period of 5.5 years. These are drastic intensity changes in the emission spectrum of the inner parts of the nebula in many wavelength ranges. Certain emission lines from the Weigelt blobs, which are gas condensations located in an equatorial disk a few tenths of an arcsecond from the central object, disappear or weaken during the event. The integrated X-ray flux from the star and the nebula is gradually building up before the event, and shows large oscillations on a 10 day scale before it finally disappears. The X-rays are absent during a couple of months before recovering to a nearly constant between- event level.

The 5.5 year period was first pointed out from the variability in the equivalent width of some emission lines[4], and based on these data an spectroscopic event was successfully predicted to appear around New Year 1998. In the coverage of the subsequent event, which was predicted to start in the beginning of July 2003, observing time was allocated on numerous telescopes to take data in different wavelength regions of Eta Carinae before, during and after the event. We had a Hubble Space Telescope Treasury Program approved to cover the event in the optical and ultraviolet region with frequent observations of the star, the equatorial ejecta and the nebula[5]. RXTE was observing on a daily basis to monitor the temporal variations of the X-ray flux. The time for the disappearance of the X-rays was correctly predicted within a few days[6].

The detailed observations of Eta Carinae during the spectroscopic event that are now available can hopefully give an answer to the question whether it is a single or binary star. The accurate period of the event supports the hypothesis of a binary system. The observations may also give some hints to what initiated the Great eruption. It might have been triggered by a close passage of a companion star in a highly eccentric orbit, since a large distance between the stars in a binary system, having such a long orbital period, would not easily trigger the eruption. Another possibility is a single star, which is bursting when it exceeds its stability limit.

The observations during the spectroscopic event might give a better understanding of the nature of Eta Carinae. They also offer a unique opportunity to study the plasma properties of the Weigelt blobs, which are equatorial ejecta that seem to host the most exciting conditions from a spectroscopist's point of view. Radiative processes, such as fluores-

[3] Gull et al. (1999)
[4] Damineli (1996)
[5] http://etacar.umn.edu; http://archive.stsci.edu/cgi-bin/proposal_search?mission=hst&id=9420
[6] M. Corcoran, http://lheawww.gsfc.nasa.gov/users/corcoran/eta_car/etacar_rxte_lightcurve/

Figure 1.1: Inverted WFPC picture showing Eta Carinae and the Homunculus. North is up and west is right. Spatial scale: 15" x 15". (J. Morse, K. Davidson, and NASA)

cence and stimulated emission, have been detected[7]. During the spectroscopic events the spectrum changes in a way that indicates abrupt changes in the plasma conditions. The indicators are different types of emission lines, whose intensity variations with time hopefully can be reproduced in a plasma model by changing various parameters. That would result in a better understanding of both the radiation field from the star, which seems to be blocked out for some time, and the radiative processes within the blobs. The vicinity of the star also hosts filament structures, which emit peculiar spectra. One of these, called the *strontium filament*, shows a spectrum completely different from what has been observed from other part of the nebula. Among other lines, we detected forbidden lines of [Sr II], which to our knowledge have not been observed before in any astrophysical spectrum.

[7] Johansson & Letokhov (2003)

The physical properties of the Weigelt blobs are ideal to produce forbidden lines of heavier elements. Forbidden lines are transitions between atomic energy levels of the same parity, and they are rarely seen in other locations than dilute astrophysical plasmas. This is because the upper levels of the transitions are sensitive to collisions and are "destroyed" in laboratory sources. Forbidden lines of [Fe II] were first identified in the spectrum of Eta Carinae[8], only a few months after Bowen [9] had solved the longstanding problems with nebular lines and classified them as forbidden transitions in doubly ionized oxygen.

Forbidden lines originate from metastable levels, which have lifetimes of the order of 1 second compared to 1 nanosecond for ordinary atomic states. The long radiative lifetime makes the levels sensitive to deexcitation by collisions, and they can therefore be used for density diagnostics of the plasma. They can also be used to determine the plasma temperature and the abundance of different chemical elements. These measurements require a knowledge about the transition probability of the forbidden lines, i.e. the probability for an excited atom in a metastable state to decay by radiation to a lower level. To meet these atomic data needs, lifetime measurements of metastable states were initiated within the FERRUM project[10]. Because of the long lifetime the ions must be kept in a low-density environment in the laboratory to prevent them from being deexcited by collisions. Our measurements have been performed in an evacuated storage ring, the CRYRING, at MSL in Stockholm. However, in order to get the transition probabilities from the lifetimes we also need to measure relative intensities of the forbidden lines, which cannot be observed in a laboratory source.

Not only is our understanding of Eta Carinae developing by means of laboratory measurements but we can also gain information on atoms by using the star and its nebula as a laboratory. The conditions occurring in astrophysical plasmas can not always be created in a laboratory, and some atomic parameters are thus best measured by studying stars and nebulae. We used the Weigelt blobs close to the central star as they show a rich emission line spectrum, especially in Fe II. From the observed line intensities, we could derive branching fractions (BF) for forbidden [Fe II] lines. The BF's give a measure of the relative flow of photons in each decay channel when the upper state decays radiatively. By combining the BF's with the measured metastable lifetime, absolute transition probabilities are derived.

The summary of the present thesis is outlined in the following way. The historical background and properties of forbidden lines are discussed in chapter 2. In chapter 3 we present Eta Carinae with an emphasis on the strontium filament, and we also briefly describe the $STIS$ spectrograph used for the observations. Selective photoexcitation due to wavelength coincidences is discussed in chapter 4, in particular the H Lyα pumping of Fe II. Chapter 5 deals with the measurements of metastable lifetimes using a laser probing

[8] Merrill (1928)
[9] Bowen (1928)
[10] Johansson et al. (2002)

technique on a stored ion beam. The measurements of astrophysical branching fractions (BF) for forbidden lines using gas condensations (the Weigelt blobs) in the Eta Carinae nebula are described as well as the procedure to derive experimental absolute transition probabilities for forbidden lines in [Fe II].

Throughout the thesis vacuum wavelengths are used, even for wavelengths in the optical region ($\lambda > 2000$Å). This is well justified and requested by users of the Hubble Space Telescope, since it is operating in vacuum. The transition energies for forbidden lines are calculated from experimental energy levels and directly transferred to vacuum wavelengths. A common unit for energy in spectroscopy is cm^{-1}, abbreviated K (Kayser). The unit kK, sometimes used in the thesis, thus stands for 10^3 cm^{-1}.

Chapter 2

Forbidden lines

Astronomical observations may thus supplement those of the laboratory by supplying data on line emission under very low densities. The character and intensity of the incident radiation may also play an important part in the duration of various electronic states. The problem can, of course, be worked both ways, and forbidden lines may thus perhaps yield information concerning conditions in the stars.

Paul W. Merrill, February 1928

In this chapter the properties of parity forbidden lines are discussed, first their discovery and identification in astrophysical spectra and then the atomic parameters of relevance, lifetime and transition probability.

2.1 Historical background

In the early days of spectroscopy the chemical elements present in stars and nebulae were identified by comparing the spectrum of the astrophysical source with individual spectra of the elements as recorded from laboratory sources. We use the same method today but the techniques are refined. Many absorption lines in spectra of the sun and stars were successfully identified by this comparison long before quantum physics had explained the secret behind the formation of monochromatic spectral lines. The situation with the

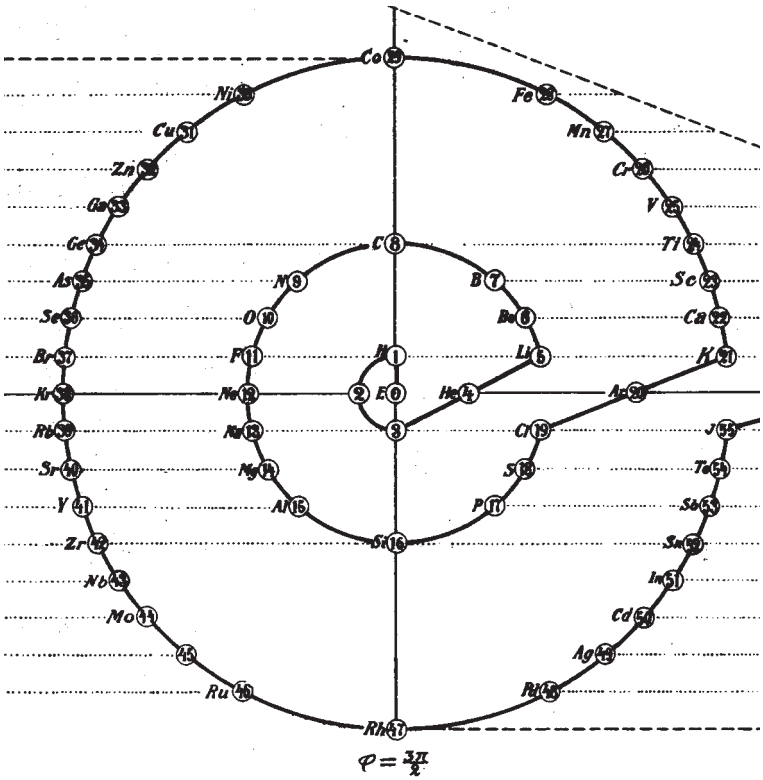

Figure 2.1: Rydberg's periodic table of the elements. In the center is the electron and between hydrogen (1) and helium (4) there are two holes (2 and 3) in which Rydberg placed two elements called Coronium and Nebulium (Rydberg 1913).

emission lines observed in spectra of nebulae was quite different, since about half of the observed optical lines remained unidentified for decades after their detection. The wavelengths of the lines observed did not match the wavelengths of any lines seen in laboratory spectra. Other strong optical emission lines were observed during a solar eclipse in 1868, and they were ascribed to the solar corona (see e.g. Hearnshaw 1986). They could not be observed under normal conditions but appeared when the solar disk was masked by the moon. Not a single one of the 22 observed corona lines could be identified. One of the many people trying to explain the corona lines was Rydberg in Lund, better known for his work on spectral regularities and the Rydberg constant. In fact, Rydberg's great project was to put together a periodic system of the elements, and his spiral version is shown in Fig. 2.1. He had two empty spots between hydrogen and helium, where he placed the elements Coronium and Nebulium, responsible for the corona and nebular

lines, respectively (Rydberg 1913; Pauli 1955). Rydberg's idea might originate from the fact that helium was discovered in the sun before it was produced in a laboratory in Uppsala (see e.g. Hearnshaw 1986). However, the idea about particular elements behind the unknown lines was later rejected.

From other emission lines observed in the nebular spectrum, belonging to H, He, C, N and O, it was expected that the unidentified lines were transitions from a light element. However, the knowledge of atomic structure did not leave any openings for any missing elements. It was also realized that the unidentified nebular lines did not belong to the same element. Based on these facts Russell et al. (1927) concluded that the lines "*must be due not to atoms of unknown kinds but to atoms of known kinds shining under unfamiliar conditions*", and they pointed out that the low number of collisions in a low density environment could be the reason. This led Bowen to conclude that these were "forbidden lines", i.e. transitions from metastable states (Bowen 1928). The strongest nebular lines were transitions between metastable states in doubly ionized oxygen, O III, a spectrum Bowen himself had analysed in the laboratory.

The identification of forbidden nebular lines by Bowen led Merrill (1928), just a few months later, to identify a set of forbidden [Fe II] lines in the spectrum of Eta Carinae. Merrill's observation of [Fe II] lines in the integrated spectrum of Eta Carinae implied that the object not only consisted of a hot star but also contained nebular regions. Recent HST observations in high spatial resolution reveal that [Fe II] lines are formed in gas condensations located only a couple of light-days from the central star. The condensations are called the Weigelt blobs (Weigelt & Ebersberger 1986; Zethson 2001) after the discoverer, who managed to detect them using speckle interferometry. These blobs are one of the best spatially well-defined locations to study [Fe II] lines, and I have used them in this thesis to derive absolute A-values for forbidden lines in Fe II (see Ch. 5).

If the speculations about the plasma conditions in planetary nebulae led to the explanation of the nebular lines, then the situation for the corona lines was more or less the opposite. From an atomic physics point of view Edléns (1943) interpretation of the corona lines was similar to Bowen's explanation of the nebular lines, but it led to unbelievable conditions in the corona itself. Grotrian (1939) noted that there was a coincidence between the transition energy of two of the coronal lines and the fine-structure splitting in the ground terms of Fe X and Fe XI. The splitting in Fe X, between $^2P_{3/2}$ and $^2P_{1/2}$, matched the λ6374 line, and $^3P_2$–$^3P_1$ in Fe XI matched the λ7892 line. This "*gave the impulse to a systematic search for analogous term separations*" and led Edlén to identify the coronal lines with forbidden transitions in highly ionized iron group elements, viz. transitions between the fine-structure levels within the ground term of highly ionized Fe, Ca and Ni (Edlén 1941, 1943). Edlén's conclusion that the temperature in the corona could be several hundred thousand degrees was in total disagreement with the general conception that the temperature far out in the corona should be much lower than the solar surface temperature (which is roughly 6000K).

2.2 Forbidden lines as a diagnostic tool

The upper levels of forbidden transitions are called metastable states. They have long lifetimes, of the order of seconds, compared to ordinary excited states with lifetimes in the nanosecond regime. In laboratory plasmas and stellar photospheres the particle density is so high that the probability for collisional deexcitation of atoms in metastable states is higher than the probability for a radiative decay. In other words, the time between collisions in the plasma is much shorter than the radiative lifetime of a metastable state. In dilute astrophysical plasmas with a large volume and low particle density, such as planetary nebulae and gas clouds around stars, the probability for collisions is low and radiation from forbidden lines is observed.

Forbidden lines are often used as a diagnostic tool in the analysis of nebulae and other thin astrophysical plasmas. Without detailed modelling they can give estimates of physical parameters such as temperature and density by measuring intensity ratios of certain pairs of lines. Parameters such as geometry or abundance do not need to be known since just the ratios between lines from a single ion are compared. Often the lines are not widely spread in wavelength which means that the effect from reddening is small.

Two levels with different excitation energy, e.g. lines from different terms, can be used for temperature determination. The difference in energy makes the relative excitation by collisions sensitive to the temperature. In the low density regime, where the time between collisions is much longer than the radiative lifetime, the levels are deexcited by emission of photons before being quenched. The line emission from each level is then only dependent on the excitation of the two levels which can be expressed as a function of atomic parameters and the temperature. For higher densities, the collisional deexcitation plays a role and has to be taken into account. Then there is a slight dependence on the line ratios from the electron density, n_e, and this has to be known to an approximate value.

If the two upper levels in a pair of forbidden lines have about the same excitation energy (e.g. two fine-structure levels) they can be used for determination of the electron density. For a low density, the dominating deexcitation process is the radiative decay. The observed line intensity is then determined solely by the rate of excitation. For two fine structure levels, the relative excitation rate is proportional to the statistical weight, so the observed intensity (in number of photons) is proportional to the ratio of the statistical weights, $n_1/n_2 = g_1/g_2$ (Osterbrock 1989). For high densities there is a Boltzmann distribution and the collisional excitation and deexcitation are equally efficient. The number of states deexcited by radiation, before the state is quenched, is proportional to the A-value. The intensity ratio is proportional to $g_1/g_2 \cdot A_1/A_2$, where A_i is the Einstein coefficient. Observed intensity ratios in the range between the extreme cases give a measure of the density of the plasma.

As has been discussed above, the density region where the lines can be used for diagnostics is an intermediate region between the extreme values for low and high density. This is determined by the competition between the radiative and the collisional deexcitation of the excited levels and is dependent on what ion is used. Different lines have different critical densities, which is the density above which the collisional deexcitation is non-negligible, and they are possible to be used as diagnostic lines. Most nebulae show strong, forbidden lines from a number of ionization stages in light elements like C, N, O. The ions of these elements have a relatively simple atomic structure and the wavelengths of the forbidden lines are in the optical region. They are therefore suitable for diagnostic purposes, since a few strong lines in the optical region dominate the spectrum and there are only a few decay channels from each level.

Since forbidden lines have low transition probabilities they are not affected by self absorption. The radiation in a forbidden line can thus escape from a nebula much easier than in an optically thick resonance line, which might be reabsorbed many times within the nebula. Forbidden lines can thus also play an important role in the cooling of nebulae (Osterbrock 1989).

2.3 Radiative lifetimes and metastable states

Excited states of an atom(ion) decay radiatively, i.e. by sending out photons, if the atom(ion) is not perturbed by interacting fields or particles. The expected time in the excited state, i.e. until the state decays radiatively, is called the radiative lifetime. The magnitude of the lifetime is determined by the number and individual rates of the decay channels down to lower states. The radiative lifetime, τ_i, for a state i is defined as

$$\tau_i = \frac{1}{\sum_k A_{ik}},$$

where A_{ik} is the transition probability for the transition from level i to k. All decay channels from a given upper level are not equally probable. The level is said to combine strongly or weakly with different lower states, i.e. have a high or low transition probability, respectively.

The transition probability (transition rate) or line strength is one of the important atomic parameters when using forbidden lines for plasma diagnostics. The expression for transition probability can generally be written proportional to $|< i|O|f >|^2$, where the operator O connects the initial state, i, and the final state, f (see e.g. Cowan 1981)[1]. For electric dipole radiation (E1), which is generally the dominating type of radiation, this

[1]The theory for radiation and transition probabilities is given in a number of text books and can be found in e.g. Thorne et al. (1999); Cowan (1981); Sobelman (1979). The derivation of transition probability for forbidden lines is also found in Garstang (1962); Shortley (1940)

operator is given by e**r**, and the corresponding transition probability is A$\sim 10^8$ s^{-1}. The E1 radiation connects states with opposite parity, i.e. an odd-parity level only decays to an even-parity level and vice versa. This parity rule comes from the fact that the operator e**r** itself has odd parity. The strongest E1 transition(s) normally observed in an atomic spectrum connects the ground state with one (or more) of the lowest levels of opposite parity. This transition(s) is called the resonance line(s).

In most elements more than one of the very lowest energy levels are of the same parity. The exceptions are in principle the rare gases, the alkali- and alkaline earth elements, with closed shells or with one or two s-electron(s) outside closed shells. For example, in the complex structure of Fe II the lowest 63 levels are of even parity, and the lowest odd-parity level has an energy of almost 5 eV. These even-parity metastable levels cannot decay by E1 transitions, as they require a parity change. However, both electric and magnetic multipole radiation is possible, and besides E1, magnetic dipole (M1) and electric quadrupole (E2) transitions have the highest probability. Since the operators for M1 and E2 do not include a parity change, M1 and E2 transitions connect states of the same parity, which opens radiative decay channels for the metastable states. These transitions are in astrophysics called "forbidden lines". Thus, the lowest levels in Fe II described above can decay by M1 and E2 radiation as forbidden lines. The transition probability for M1 and E2 transitions are of the order A$\sim$1 s^{-1} and for low ionization stages many orders of magnitude lower than E1. If an excited level can decay in an E1 transition, the M1 and E2 emission will be of negligible strength. But if no E1 decay channels are available the "forbidden" M1 and E2 lines dominate and are observed in spectra of dilute astrophysical plasmas.

In addition to the parity restrictions, selection rules for the change in the total angular momentum J apply for the different types of radiation. The properties for E1, M1 and E2 transitions are given in Table 2.1. The first set is sometimes referred to as "rigorous selection rules", and they follow as conditions in the quantum mechanical treatment of the interaction between an atom and electromagnetic radiation (Garstang 1962). These conditions are independent of the coupling scheme used for describing the atomic structure. The conditions associated with the various models (coupling schemes) that are used to describe the atom also generate sets of selection rules. For example, the selection rules in the LS coupling model put constraints on the change of total orbital and spin angular momenta, L and S, and they are given in the lower section of Table 2.1. LS coupling is often a good approximation for the lowest configurations, and the selection rules may therefore be valid for the forbidden transitions. However, in general, different parts of the total energy level system in complex spectra, such as Fe II, are represented by different coupling schemes. One should therefore be very careful in interpreting the LS notations of the energy levels, often used in the literature, as representative from the physics point of view.

In the absence of configuration interaction (CI) the restrictions Δn=Δl=0 also apply to

E1	M1	E2
	Rigorous selection rules	
parity change	no parity change	no parity change
ΔJ =0,$\pm$1	ΔJ =0,$\pm$1	ΔJ =0,$\pm$1,$\pm$2
(0 $\nleftrightarrow$ 0)	(0 $\nleftrightarrow$ 0)	(0 $\nleftrightarrow$ 0, 1/2 $\nleftrightarrow$ 1/2, 0 $\nleftrightarrow$ 1)
	LS selection rules	
ΔS=0	ΔS=0	ΔS=0
ΔL=0,$\pm$1	ΔL=0	ΔL=0,$\pm$1,$\pm$2

Table 2.1: Selection rules for electric dipole (E1), magnetic dipole (M1) and electric quadrupole (E2) radiation.

M1 radiation and limit transitions to occur only within the same configuration. Combined with the LS rules from Table 2.1 (ΔS=ΔL=0) this means that only transitions between the fine structure levels within a given term are allowed (or in the case of equivalent electrons, between terms having the same value of L and S). However, configuration interaction and/or deviations from the LS approximation make other transitions observable as well. For the case ΔJ=0, this is a transition where the initial and final level are the same level and no real transition could be possible. But, if fractions of a state are mixed into two levels a M1 transition can appear between the levels although this basically is an intra-state transition.

There are cases where an atomic level cannot decay by any of the multipole transitions discussed so far: E1, M1 and E2. One extreme example is found in the spectrum of Yb II, where a closed 4f shell and a 6s electron form an even-parity $^2S_{1/2}$ ground state. The first excited state is formed when one of the 4f electrons is excited to 6s, closing the 6s shell. The excited state is thus a hole in the 4f shell, which forms a ^{2}F term of odd parity. The J=7/2 level can energetically only decay down to the ground state, which means a parity change and a large change in J (ΔJ=3). Such a transition is not covered by the selection rules given in Table 2.1, and it is only possible to occur with electric octopole (E3) radiation. The corresponding transition probability is extremely low, which is verified by measurements, and the radiative lifetime of the $^2F_{7/2}$ level is about 10 years (Roberts et al. 1997).

In astronomical literature forbidden lines are denoted by the spectroscopic notation of the spectrum of the element (i.e. Fe II for singly ionized iron) inserted in brackets, e.g. [Fe II] for forbidden lines of Fe II. They should definitely not be confused with intercombination (IC) lines, denoted by a right bracket, e.g. CIII] and mentioned above, even if the latter are sometimes referred to as semi-forbidden lines. An IC-line includes a change of the spin ($\Delta S \neq 0$) and has often a low transition probability in light elements, where the LS coupling approximation is valid. Thus, the occurrence of IC lines in a high-density laboratory light source just indicates a departure from LS coupling, whereas the occur-

rence of IC lines in an astrophysical plasma may imply a low density. Therefore, they are sometimes called semi-forbidden lines.

Chapter 3

Eta Carinae

The spectral analysis of Eta Carinae in this thesis is based on spectra from The Hubble Space Telescope (HST). We have used the Space Telescope Imaging Spectrograph (STIS) onboard HST, and the instrument is briefly described in order to give a background and insight of the shape and composition of the different spectra and plots presented in the thesis. The overall structure of the object and its surroundings is also described in the present chapter. A particular region of the nebula, called 'the Strontium Filament', is discussed in detail.

3.1 Eta Carinae, the object

Eta Carinae is one of the most massive stars known in the Galaxy. The stellar mass is not well known but estimated to be more than 130 solar masses, and the luminosity is estimated to be $5 \cdot 10^6$ times the solar luminosity (Davidson & Humphreys 1997). The distance to the object is about 7500 light years. In the 1840's Eta Carinae experienced a major outburst, referred to as the Great Eruption. The visual magnitude increased to m_v=–1, and Eta was the second brightest star in the sky, only surpassed by Sirius. After 1856 it faded and became more or less invisible around 1870 at seventh or eighth magnitude. The star brightened again during a smaller eruption in the 1890's, but, probably due to circumstellar dust, it did not reach the brightness observed during the Great Eruption. The present value of the visual magnitude is $m_v \sim 5$, making the object barely visible to the naked eye.

Pictures of Eta Carinae today show that the star is surrounded by a bipolar nebula, where the two lobes have a diameter of about 8.5 arcsec (see Fig 3.1). The nebula, called the

Homunculus, is thought to consist of the two hollow lobes, each with about a solar mass of dust and gas. They expand at velocities indicating that the matter was ejected during the Great Eruption. Recent HST studies indicate that there is a *Little Homunculus* residing inside the nebula. It has the same shape but a smaller size and it is thought to have been produced in the smaller eruption in the 1890's (Ishibashi et al. 2003). Larger thin gas clouds outside of the Homunculus indicate that eruptions have taken place even before 1840. Around the waist of Eta Carinae a partial disc-like structure is observed. This is also thought to be produced during the large eruptions or smaller ejections. Spectra taken through a slit placed across the disc show many different components, which have different radial velocities (different Doppler shifts in the lines) and even different chemical compositions (Zethson et al. 1999, Paper V).

One of these components (blobs, filaments, gas condensations), the strontium filament, is especially studied in this thesis (Papers III-V). In the spectrum of the Sr filament we have identified forbidden Sr II lines, [Sr II], and this is the first detection of [Sr II] in any terrestrial or astrophysical light source. The Sr filament shows a completely different spectrum compared to other regions in the whole nebula, and it is discussed in more detail in Sec. 3.3 below. Close to the star there are also gas condensations, whose spectra contain more than 2500 emission lines of various kinds. For example, there are strong [FeII] and <FeII> lines, i.e. forbidden and fluorescent Fe II lines, respectively, where the latter are pumped by H Lyα (Zethson 2001; Johansson & Hamann 1993). The plasma conditions in the blobs - low density, strong radiation fields - make them a good astrophysical laboratory to study forbidden and fluorescent lines. As discussed in Ch. 2 forbidden lines are formed under low density conditions and they are not easily generated in a laboratory plasma. Thus the [FeII] lines observed in the blobs of Eta Carinae have been used in this thesis to measure branching ratios and derive absolute transition probabilities of forbidden lines. This is discussed in more detail in Ch. 5 and Paper VII.

In addition to the large eruptions observed in the 19th century the spectrum of Eta Carinae implies smaller activities on a much shorter time scale. Damineli (1996) discovered a 5.52 year period in the variation of some optical emission lines, e.g. HeI, which he associated with an orbital period for a binary star system. During the major part of the period the spectrum is unchanged but for a short time, called *the spectroscopic event*, a large activity occurs. The spectra of the star and the blobs change drastically in many wavelength regions during the event, which lasts for a couple of months. From previous events and the 5.52 year period the latest event was predicted to start in late June of 2003. Daily x-ray observations using RXTE (Corcoran 2003) showed large oscillations (with a period of $\approx$10 days) and an average increase in the X-ray flux during the first half of 2003. Suddenly, the X-ray flux dropped around June 15 and was nearly absent by July 1. After about 60 days of calm at a very low background level the X-ray flux started to increase again. Whether the spectroscopic event is a sign of an eclipse of a binary or a periodic outburst from a single star is not clear, but the analysis of the large amount of spectroscopic data collected during 2003 may give an answer. It seems that the fast oscillations

in the X-ray flux and the sharp periodicity favour a binary star model.

Besides the changes observed in the integrated X-ray flux the H Lyα excited Fe II and Fe III lines in the Weigelt blobs also show dramatic changes and disappear during the spectroscopic event. The same is true for intercombination and forbidden lines of multiply ionized atoms, e.g. Si III] and [Ne III] (Zethson 2001; Davidson et al. 1999). Detailed analyses are in progress but the conclusion is that the high-energetic part of the ionizing and exciting radiation from the star is blocked and does not reach the blobs.

3.2 The Space Telescope Imaging Spectrograph

The spectra of Eta Carinae used in this thesis are taken with the Space Telescope Imaging Spectrograph (STIS) onboard Hubble Space Telescope (HST). This instrument is very suitable for spatially resolved spectroscopy of Eta Carinae. The access to good spatial as well as spectral resolution makes it possible to study the different parts of the nebula. Spectra from such regions as the Weigelt blobs, the central star and the Strontium filament can then be studied and analysed separately. An advantage of a telescope above the earth's atmosphere, compared to ground based observatory, is the absence of air in the line of sight. This fact makes it possible to study the ultraviolet region as well as it provides good spectra in the far-red region, where absorption from atmospheric molecules is severe.

STIS can basically be used in two different modes for recording spectra of stellar and nebular regions:

- High spectral resolution (R$\sim$200 000) echelle mode. This is only accessible in the ultraviolet region. A medium resolution mode is also available.
- Medium spectral resolution (R$\sim$5 000–10 000) long slit mode. The two-dimensional CCD detector is in this case used for collecting spatial information along the slit in one dimension and spectral data for each location in the other dimension. A low resolution mode (R$\sim$ 750) is also available. The spectral range covered is 1635-10140Å.

The long slit medium resolution mode is ideal for studying extended objects like Eta Carinae. It is possible to simultaneously observe spectra from the different spatial locations along the slit in a single observation. This mode has been used for the Sr filament observations, discussed in Sec. 3.3 and Paper III and V. The spatial extent and the intensity of the different lines along the slit can be measured and give information about the size of different nebular clouds as well as varying excitation and velocity conditions within them. An example of a three dimensional spectrum is given in Figure 3.1. The y-axis gives the spatial coordinates, the x-axis the spectrum wavelength and the z-axis the

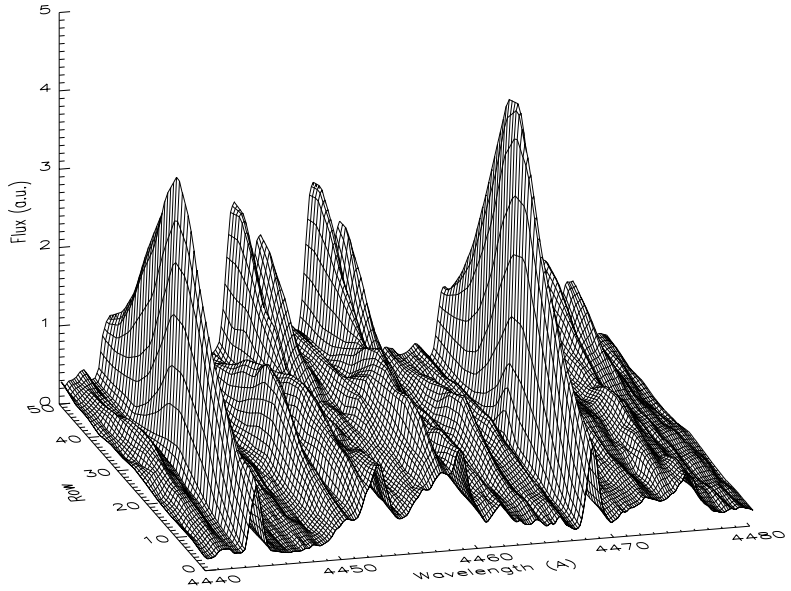

Figure 3.1: Two dimensional spectrum of Eta Carinae with spectral dispersion along the x-axis and spatial distribution along the y-axis. The lines peaking in the middle (e.g. 4444 and 4468 Å) of the spatial scale are from the strontium filament whereas the lines peaking at the border (e.g. 4453 and 4458 Å) are from another spatial location. The spatial extent is about 1".

intensity distribution. The difference in appearance of lines from separate regions can be seen in the picture. The Ti II lines from the Sr filament at 4444 and 4468 Å peak in the middle whereas the [Fe II] lines at 4453 and 4458 Å originate from another spatial region and have a different spatial structure. The intensity in each row contains the spectral distribution in a spatial location and for more detailed spectroscopic analysis an extracted spectrum from one or more rows is used. (Examples of extracted spectra are given in Paper V). The spatial resolution for the optical region is of the order of 0.1" (Woodgate et al. 1998).

The grating modes used are denoted G230MB, G430M and G750M, and they cover together the wavelength region 1635-10140Å in 29 grating positions. A single exposure with any of these gratings only covers some hundred Ångströms but tilting the grating makes it possible to cover the whole region by making about 10 exposures with each

grating. For the long-slit observations different slit apertures are available, and we have used an aperture of 52"×0.2" in order to get enough flux and still have a reasonable resolution. With this aperture the exposure time was about 200 s for each grating setting, whereas the narrower apertures would have required much longer exposures.

Detailed information about the settings for the observations are given in Table 1 in Paper V and a more complete description of STIS is given by Leitherer (2001); Woodgate et al. (1998); Kimble et al. (1998).

3.3 The spectrum of the strontium filament

As described in Paper III the strange emission lines from the region called the strontium filament were discovered during a mapping project of the Homunculus of Eta Carinae (Gull & Ishibashi 2001). The nebula was observed with the long slit of STIS in two wavelength regions: one centered at 6768 Å, which contains Hα, and the other centered at 4961 Å, which contains Hβ. Additional observations were made in March 2000. The slit is 52" long and it extends over the whole nebula. Observations were made with the slit oriented almost along the polar axis of the nebula and with an offset of 0.5" between the subsequent observations in the 6768 Å setting and 0.25" in the 4961 Å setting. The observations resulted in a set of spectra that covers the whole nebula in these wavelength regions. In one spatial location, 1.5" NW of the central object, the spectrum differed remarkably from other spectra, and emission lines were seen that had not been observed in any other region. Two of the lines were identified as forbidden transitions of singly ionized strontium, [Sr II] - the first known identification of these lines in any light source (Paper III). The detection of the [Sr II] lines was totally unexpected from an astrophysical point of view. Other lines, identified as [Fe I] and [Ti II], are also somewhat unexpected and not seen in other gas condensations.

Further HST/STIS observations of the Sr filament, in total covering the spectral range from 1635 to 10140 Å, have subsequently been obtained on different dates and with different slit orientations. Below 2000 Å there is nearly no emission at all, and the region 2000-3000 Å is heavily affected by superimposed absorption. Above 3000 Å the spectrum shows numerous emission lines, both allowed and forbidden. Emission lines from other spatial regions along the line of sight contribute as well to the total spectrum recorded of the region including the Sr filament. However, due to different spatial and spectral shapes, the lines associated with the Sr filament itself can be separated from the foreground and background lines (see Figure 3.1). There are cases where the same atomic transition is emitted from a number of spatial locations along the line of sight, and in these cases it can be difficult to determine whether there is a contribution from the Sr filament.

In total we manage to identify around 600 emission lines that are formed in the Sr fil-

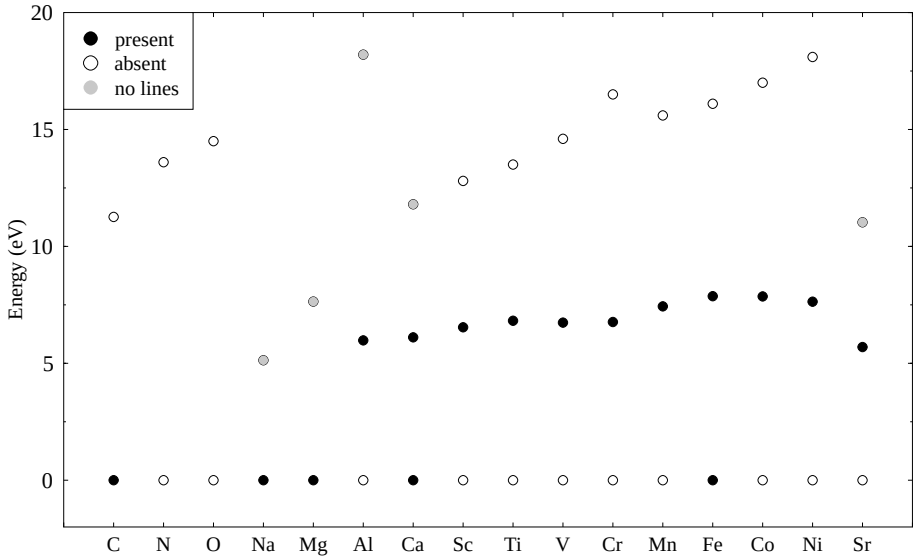

Figure 3.2: The lowest ionization stages for observed elements represented by the ground state energy of each ion. (zero = ground state of the neutral atom.) Black dots mark ions that are seen, white dots mark ions not seen and the grey dots mark ions not expected to be seen although they are present in the plasma.

ament. They are listed in Paper V, where we can see that lines from TiII, VII and FeI dominate the spectrum. In addition, lines from CI, MgI, AlII, CaI, CaII, ScII, CrII, MnII, FeII, CoII, NiII and SrII are observed. Strangely enough, we do not see any lines from the cosmically abundant light elements H, He, N or O in this region. Neither do we succeed in identifying any heavier elements than Sr with confidence.

A number of fairly strong lines remain unidentified. Some of these coincide in wavelength with Y II but since other prominent, and equally probable, lines are missing in the spectrum we hesitate to present them as positive Y II identifications. Three unidentified lines coincide in wavelength with Zr II, two of which are strong resonance transitions.

3.3.1 The influence of atomic structure on observed line densities

In Figure 3.2 we try to summarize graphically the various elements that have been detected in the Sr filament and also illustrate the absence of some elements with high cosmic abundance. Thus, we have marked all elements at various ionization stages that have been

observed. The ions that have not been observed are divided into two categories:
1) the ions that have lines in the observed region and therefore are possible to detect and 2) the ions that have no lines in the observed region and therefore are not possible to detect. The reason why the ions in the latter category cannot be observed is that the lines either fall in an unobserved region (far UV or IR) or that the excitation energy is too high for the appropriate levels to be populated. For the ions detected we observe lines from energy levels having an excitation energy of maximum 6-7 eV ($\sim$48-56 000 cm^{-1}). Thus, the atomic structure of the atoms and ions has to be considered before drawing any conclusions about their presence in the astrophysical plasma studied.

The number of lines observed in a stellar spectrum is also dependent on the atomic structure. A text-book case in most stars is neon, which has about the same cosmic abundance as iron. The resonance lines appear below the Lyman limit and the optical lines require an excitation energy of more than 16 eV. Sr II, which is a one-electron system and of relevance here, can only contribute five lines (three allowed and two parity-forbidden) in the spectrum of the Sr filament, if we assume a highest excitation energy of about 6 eV. Two additional allowed lines appear outside the wavelength region studied. The next higher level, 6s $^2\mathrm{S}_{1/2}$, has an energy of 6 eV and no emission lines from this level have been observed. The structure of Sr^+ is similar to the structure of neutral alkali metals and singly ionized alkaline earth-like elements. The situation for Ti II is different, since the transition elements have two or three open subshells. This generates a more complex structure, and consequently there are about 150 Ti II lines observed in the Sr filament. The level population is then distributed over many energy levels and the total flux thereby shared by a large number of transitions, making each line relatively less intense.

In Figure 3.3 the TiII lines in the range 3 000-10 000 Å are displayed in a diagram where the excitation energy of the upper level is plotted versus the gA-value. The grey dots mark all predicted transitions and superimposed in black are shown the emission lines observed from the strontium filament. The plot for Sr II is basically the same, except that the wavelength range is extended to 11 000 Å in order to include the 4d-5p lines (of which only one line is within the observed spectral region). From the plots we can see the difference in line richness between spectra of a "simple" atomic system, Sr II, and a more complex system, TiII.

3.3.2 Plasma properties

In the spectrum of the Sr filament we observe numerous lines that can be used to probe the physical properties of the filament. As discussed in Sec. 2 forbidden lines are often useful for diagnostics. Even if Sr II, like Ca II, has an alkali-like structure there are two metastable states due to the fact that the 4d electron is more tightly bound than the 5p electron. Thus, the ground state of Sr II is 5s $^2\mathrm{S}_{1/2}$, the metastable levels are 4d $^2\mathrm{D}_{3/2,5/2}$, and higher up the 5p $^2\mathrm{P}_{1/2,3/2}$ levels of opposite parity are located. The

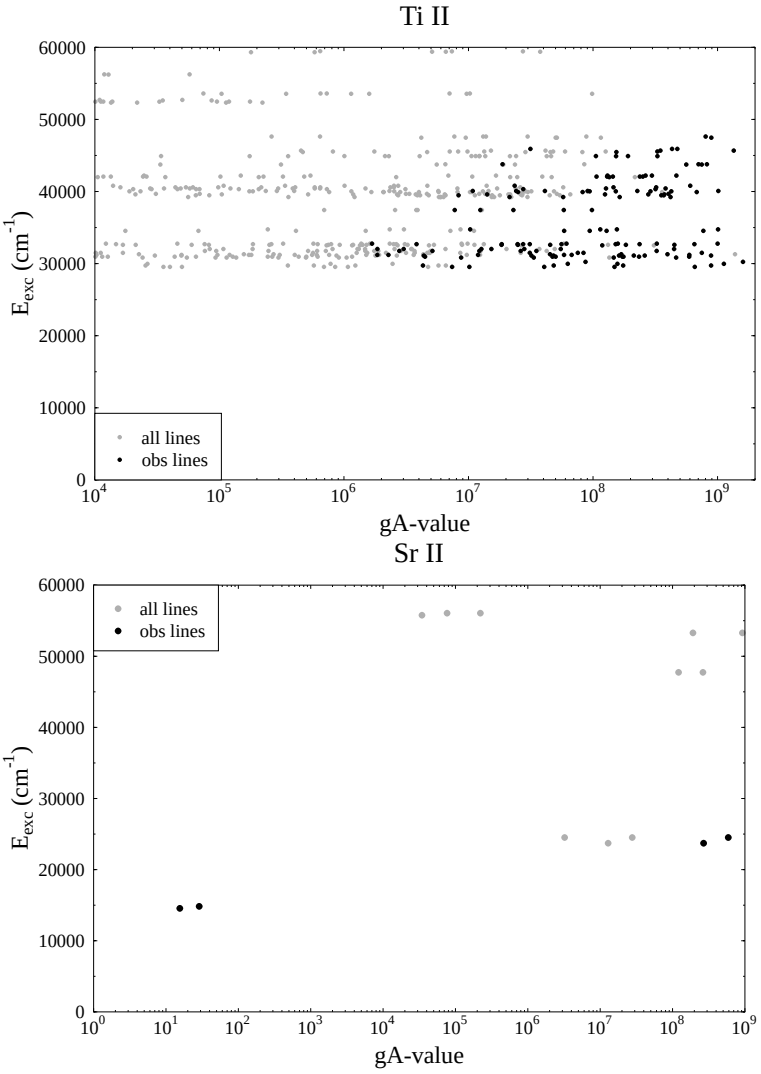

Figure 3.3: Lines from TiII (left panel) and SrII (right panel) in the region 3000-10000 Å for TiII and 3000-11000 Å for SrII. All possible lines are plotted in grey and the lines observed in the spectrum are overplotted in black. The difference in atomic structure is obvious. Note the different x-scales. The forbidden lines of [TiII] are not included.

decay from a 4d to a 5s orbital generates forbidden lines. The only lines observed in the Sr filament are the 5s-5p resonance lines at λ4077, 4122 and the forbidden 5s-4d lines

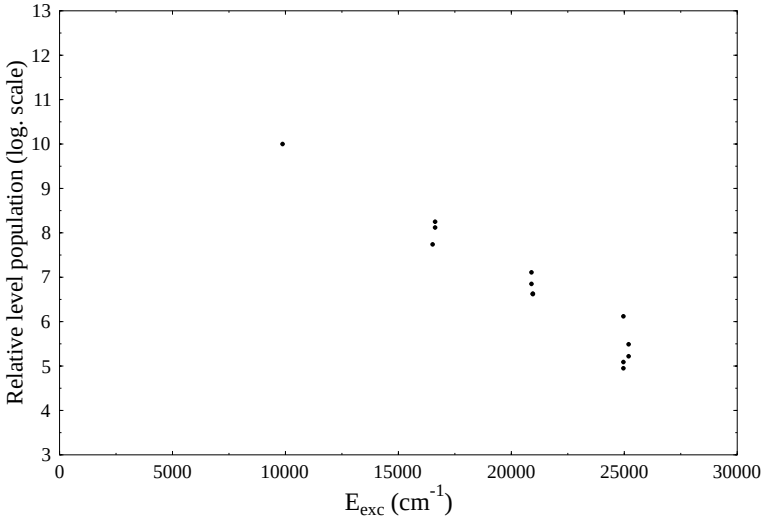

Figure 3.4: On the vertical axis is given $\ln[(I_{ij}/\epsilon_{ij})/(A_{ij} \cdot g_i)]$, i.e. the relative level population, and on the horizontal the excitation energy. The strongest transitions in [Ti II] are included in the plot.

at λ6740, 6870. Even if we extended the observations to 10140 Å we do not observe the allowed 4d-5p line at 10039 Å. This is probably due to a combination of low efficiency of the detector in this wavelength region and a low transition probability. The other two 4d-5p lines have wavelengths of 10330 and 10917 Å and are outside the observed wavelength region. The intensity ratio of the two forbidden lines is sensitive to the electron density as described in Paper IV. The measured intensity ratio indicates an electron density close to $10^7 \mathrm{cm}^{-3}$.

The number of metastable states increases rapidly with the number of valence electrons in complex spectra of iron group elements, where the three lowest configurations are combinations of d- and s-electrons, having the same parity. Ti II is the dominating contributor to the spectrum of the Sr filament, and we see forbidden lines from all metastable energy levels, which can generate lines in the observed wavelength region.

In the high density regime, the level populations are determined by collisions and follow a Boltzmann distribution, $N_1/N_2 = g_1/g_2 \cdot \mathrm{e}^{-\Delta E/kT}$. From this, an excitation temperature can be derived from the relative level population, assuming a Boltzmann distribution. In Ti II, the energy of the metastable levels is in the range 10 000-25 000 cm^{-1}, which makes it possible to check the consistency using many levels with a spread in energy. Ishibashi et al. (2003) derived the temperature for the *Little Homunculcus* with this approach using [Fe II] lines. The fraction of atoms in a certain state decaying radiatively

before being collisionally deexcited is proportional to the gA value for the observed line. The population of a level is then proportional to the observed number of photons normalized to this fraction.

By comparing the observed emission (in units of number of photons) with the transition probabilities the relative level population can be estimated. In Figure 3.4 this ratio is plotted for the different levels in Ti II as a function of excitation energy using the strongest lines. As can be seen from the figure the points fall on a straight line. From the slope an excitation temperature can be derived if a Boltzmann distribution is assumed. The lines from the different levels fall in different regions and scattering affects the different lines unequally since blue light is scattered more than red (see Sec. 5.4 and Paper VII). When correcting for this effect, assuming a value of the visual extinction $A_V \sim 2$, a fitted line to the slope gives a value of 6000 K for the excitation temperature from the [Ti II] lines.

Chapter 4

Fluorescence

In the previous chapter we discussed the excitation and deexcitation of metastable energy levels, which produce forbidden lines in spectra of dilute plasmas. For ordinary excited levels with short lifetimes (1-10 ns) the major deexcitation process is the radiative decay. The excitation of these levels is, on the contrary, sensitive to the properties of the plasma where the atoms (ions) reside, i.e. the temperature, the pressure and the radiation field. Many emission lines observed in spectra of nebulae and other thin plasmas are thought to be formed either by collisions (mainly with electrons) or by recombination (radiative capture). However, short-lived levels can also be photoexcited, either by absorption of continuous radiation from a nearby star or by monochromatic light from strong emission lines present in the environment. The subsequent decay occurs in one or more fluorescence lines.

Thus, in the presence of strong radiation fields a non-LTE level population can be obtained in a low-density plasma due to selective photoexcitation. In this chapter we will consider two cases: Photoexcitation by continuum radiation (PCR) and photoexcitation by an accidental resonance (PAR). There will be a special emphasis on a PAR process where Fe II is selectively photoexcited by H Lyα.

4.1 Photoexcitation by continuous radiation

Some stellar spectra contain numerous allowed emission lines, where the corresponding upper level is pumped by continuum radiation from a nearby star. This is often referred to as photoexcitation by continuous radiation (PCR). Such lines are observed e.g. in satellite spectra of the symbiotic star KQ Puppis (Viotti et al. 1989; Redfors & Johansson 2000),

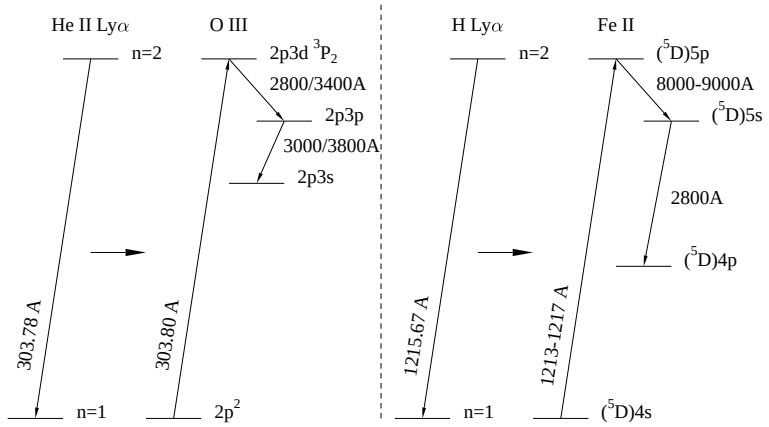

Figure 4.1: Principle for the Bowen mechanism in O III and a similar fluorescence case in Fe II.

where high-lying excited levels in Fe II are populated by absorption of UV continuum radiation from one of the stars in the symbiotic system. A large number of levels are observed having an enhanced population and all of them are photoexcited from a low level, which is verified by observed absorption lines. And, inversely, all levels having strong channels down to the lowest levels in this wavelength region show an enhanced population. The population enhancement is determined by the excitation energy of the absorbing level and the oscillator strength of the absorption line. Some radiative energy is in this way transferred from the UV continuum to optically thin fluorescent lines at longer wavelength through the line absorption.

In analyses of the abundance pattern in Active Galactic Nuclei (AGN) it has also been shown that it is important to consider PCR (Verner et al. 2003). In low resolution spectra of AGN the iron abundance is measured as integrated flux in large UV bands of the Fe II resonance region. However, this is the region where also the PCR pumped fluorescence lines appear. It is thus important to include fluorescence in the modelling of AGN since it affects the total flux in the UV region.

4.2 Photoexcitation due to an accidental resonance

In spectra of some astrophysical plasmas one can observe some of the individual transitions in an LS multiplet as strong lines, whereas other components of the same multiplet are absent in spite of a similar excitation energy. The observations clearly imply a large non-LTE distribution of the population of the energy levels. The excitation mechanism

behind this observation has to be selective with sharp resonances in the excitation cross sections. The most probable mechanism is a photoexcitation due to an accidental resonance (PAR) (Kastner & Bhatia 1986), i.e. the wavelength of a strong line coincides with the wavelength of a transition in the pumped ion. Photons from the pumping line of an abundant element in the plasma (e.g. H, He, C, etc) excite the pumped ion in the same plasma from a very low state, in general, to a higher state. When the photoexcited level in the pumped ion decays, the radiation is distributed in a number of decay channels (fluorescence lines) according to their transition probabilities. The fluorescence lines are often optically thin and can therefore easily escape from the plasma and act as a cooling agent for the gas.

The PAR process described above is often referred to as the Bowen mechanism since Bowen was not only first to identify forbidden [O III] lines (see Sec. 2.1) in nebulae but also first to explain strong nebular lines as fluorescent O III lines (Bowen 1934). All these identifications were based on Bowen's own laboratory analysis of O III. The strength of the [O III] lines in nebulae had been a puzzle and seemed to be correlated with the strength of optical He II lines (Bowen 1928). Lines from high excitation levels in O III were also observed in nebular spectra, but only from certain energy levels. Bowen noted the coincidence in wavelength between the He II line at 303.780 Å and the O III transition from the ground state $2p^2\ ^3P_2$ to the excited state 2p3d $^3P_2$ at 303.799 Å. Radiative energy can thus be transferred from He II to O III, which is excited to the 2p3d $^3P_2$ state. The most probable decay branch for this level is back to the $2p^2$ ground state with a new 303 Å photon as a result. But, there is a probability of a few percent that O III decays to 2p3p and subsequently to 2p3s resulting in emission of fluorescence lines in the 3000-4000Å region (Bowen 1934, 1935). A simplified level diagram is given in Fig. 4.1. Since the fluorescence lines are high excitation lines, and their lower states are efficiently depleted by a prompt decay down to the ground states, they are optically thin. The radiative energy can thus be transferred from the optically thick He II line to the O III lines and thereby more easily escape from the nebula.

For the fluorescence process to work efficiently a number of requirements must be fulfilled. The pumping line must be strong, i.e. have an intense radiation field. The absorption line with the coincident wavelength in the pumped ion must have a large transition probability, and the lower state a sufficiently large population. The latter is normally achieved by collisional excitation for low states in abundant ions. A complex spectrum with many energy levels is also very line rich, and there is a high probability for a wavelength coincidence to occur. An example is given in Paper II of the prominent UV 34 multiplet in Fe III, where one level is pumped and yields fluorescence in the 1914 Å line. The level z^7P_3 is pumped by H Lyα from the ground state a^5D_4, but the other levels, z^7P_2 and z^7P_4, do not show any sign of enhanced population. The pumping channels for the z^7P_2 are too far from H Lyα, the closest being at 1226 Å. The z^7P_4 has a transition at 1213 Å which is probably within the line profile of H Lyα. However, the transition probability is too low for efficient pumping, a few orders of magnitude less than for the

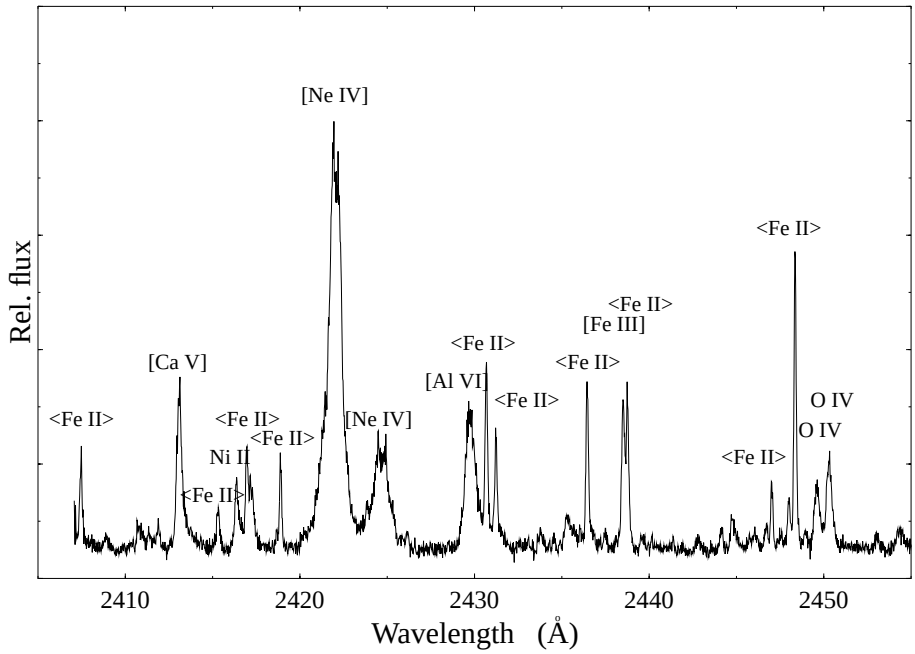

Figure 4.2: Part of the ultraviolet spectrum of RR Tel showing numerous fluorescent <Fe II> and high ionization lines.

transitions to z^7P_3. The reason for this difference is a level mixing with the close z^5P term, which does not have a J=4 level but can transfer some quintet character to the J=3 level. Thus, the z^7P_4 level has a pure septet character resulting in a low transition probability for the intercombination transitions to a^5D.

Since the time when Bowen explained the nature of fluorescence lines a number of similar processes with other elements involved have been detected. A compilation of known PAR processes, including pumping lines and pumped levels are given in Appendix A.

Fe II line emission from a number of levels at 11 eV is observed strong in a number of stars (Brown et al. 1979; Johansson & Jordan 1984; Johansson & Hamann 1993; Johansson et al. 2001, Paper I). Other levels, with similar or lower energy, do not show any emission at all. The populated levels, with configuration (^{5}D)5p, do all have strong channels down to the ground configuration (^{5}D)4s with wavelengths all within a few Ångströms from H Lyα at 1215 Å and are thought to be pumped by the PAR process. They are discussed in more detail in the section below in connection with the identification of fluorescence

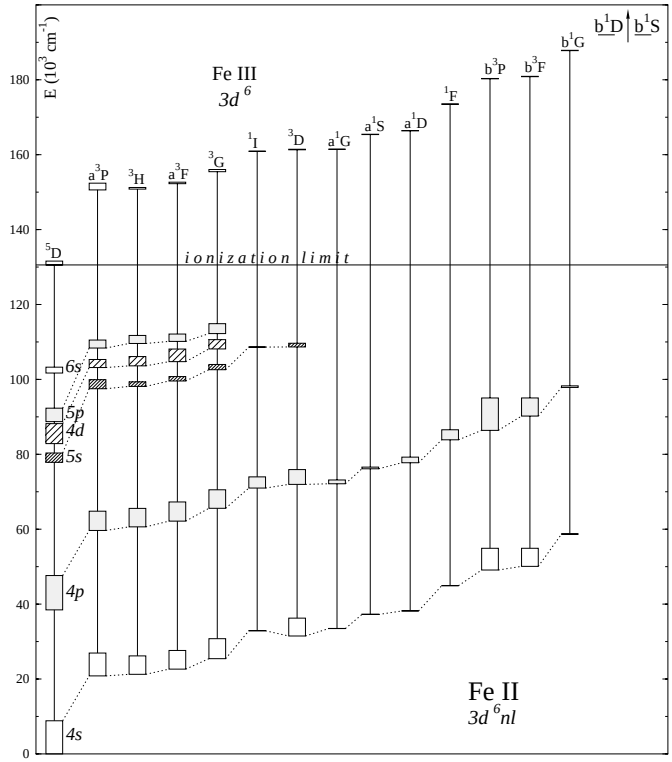

Figure 4.3: Energy level diagram on Fe II (by courtesy of Sveneric Johansson).

lines in the symbiotic nova RR Tel.

The spectrum of Cr II is also observed to show fluorescence lines pumped by H Lyα. The atomic structure of Cr II is similar to Fe II; the lowest configurations are 3d^5 or 3d$^4(^M L)nl$ in Cr II compared to 3d^7 or 3d$^6(^M L)nl$ in Fe II. The configurations 3d^6 and 3d^4 give rise to the same terms which means that 3d$^6(^M L)nl$ and 3d$^4(^M L)nl$ in Fe II and Cr II, respectively, have the same parent terms $^M L$. The energy separation in Cr II is similar to Fe II, and H Lyα matches therefore also the energy separation 4s-5p in Cr II. Infrared fluorescence lines of Cr II are seen from these levels in Eta Carinae (Hamann et al. 1994; Zethson et al. 2001).

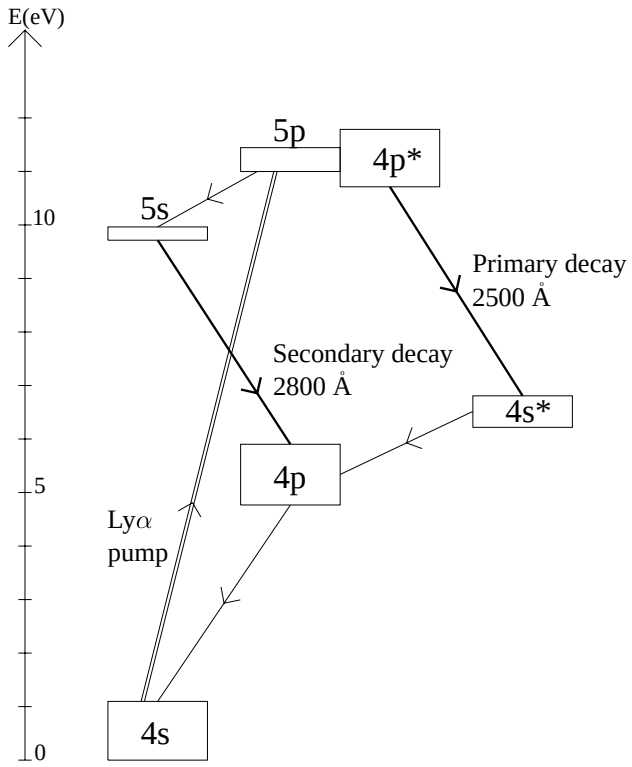

Figure 4.4: Primary and secondary UV fluorescence channels (bold lines) from Fe II levels pumped by H Lyα. (Notations: nl=(^{5}D)nl; nl^*=(b^{3}F)nl, (b^{3}P)nl)

4.2.1 Fluorescent Fe II lines in RR Tel

The continuum radiation is often weak in the ultraviolet region of symbiotic stars since the Planck radiation from the hot and the cool stars in the symbiotic system dominates at shorter and longer wavelengths, respectively. Superimposed on the weak continuum is a rich emission line spectrum, dominated by Fe II lines from high-excitation levels in addition to lines of highly-ionized light elements (see spectrum in Fig. 4.2). Many of the Fe II lines are observed from specific odd levels with an energy of about 11 eV.

All levels which show an enhanced population and fluorescence lines have a strong transition connecting to a low state. As described above, many of these coincide in wavelength with H Lyα at 1215 Å. The flux is thus transferred from H Lyα, absorbed by Fe II and reemitted in the fluorescence lines observed. The levels observed to be pumped by H Lyα

Table 4.1: Pumping lines and corresponding pumped levels in Fe II observed in the ultraviolet spectrum of RR Tel.

Pumping line (Å)	Pumped level
H Lya 1215	(b^3F)4p $^4G_{9/2}$, (^{5}D)5p $^6F_{9/2}$, (b^3P)4p $^4S_{3/2}$, (^{5}D)5p $^4D_{5/2}$, (b^3P)4p $^4P_{1/2}$, (^{5}D)5p $^4P_{5/2}$, (^{5}D)5p $^4D_{3/2}$, (^{5}D)5p $^4F_{5/2}$, (^{5}D)5p $^4F_{3/2}$, (^{2}D)4s4p(^{3}P) $^4F_{7/2}$, (^{2}F)4s4p(^{3}P) $^4G_{11/2}$
Si III] 1892	$z^4G_{9/2}$, $x^4F_{5/2}$
[Fe IV] 2835	$z^4G_{5/2}$
O III] 1661	$z^2G_{9/2}$
[Ne V] 1575	$x^4G_{7/2}$
C IV 1548	$y^4H_{11/2}$, $w^2D_{3/2}$
<Fe II> 1776	$x^2H_{9/2}$
He II 1084	$x^4H_{11/2}$, $u^2G_{9/2}$
N IV] 1487	$u^4F_{3/2}$
Ne V 1146	(^{4}G)4s4p(^{3}P) $^4H_{9/2}$
Si III 1207	(^{4}G)4s4p(^{3}P) $^4H_{9/2}$
O VI 1032	(a^3F)5p $^4D_{5/2}$
Primary decay	5s e^6D, 5s e^4D, (a^3F)5s $f^4F_{5/2}$

belong to the configurations (^{5}D)5p, (b^3P)4p and (b^3F)4p. The small energy difference between them enhances the mixing between the levels and they share some properties. This mixing is responsible for enhancing the strength of the pumping channels for the latter two configurations. Strong lines are also seen from even parity levels. These cannot be pumped directly from any of the low even parity levels but are rather populated through cascades from the H Lyα pumped levels.

The natural way for the H Lyα pumped (^{5}D)5p levels to decay is within the (^{5}D)nl system either back to 4s or via the 3-photon route 5p→5s→4p→4s where the wavelength regions for the different steps are 9000Å, 2800Å and 2500Å, respectively. The secondary decay is observed from almost all of the (^{5}D)5s levels, both from e^4D and e^6D. When decaying, the flux is spread over many channels, and the flux per transition is thus also less from levels further down in the system. But some 5s levels are fed by cascades from many upper levels which might compensate for that. The (b^3P)4p and (b^3F)4p levels have their primary decay in the ultraviolet (Fig. 4.4).

Fluorescence lines pumped by H Lyα are observed in a number of astrophysical objects. In RR Tel, strong lines from additional levels in Fe II are observed as well. In general they come from low excitation states compared to the H Lyα pumped levels. As reported in Johansson (1983, 1988) and Paper I other lines are responsible for this pumping, see Table 4.1 and Paper I, Table 1.

The pumping channels for these levels differ in wavelength, since the different (^{M}L)4p states have different energies depending on parent term, from 60 kK for (a^{3}P)4p up to almost 100 kK for (b^{1}G)4p (see level diagram on Fe II in Fig. 4.3). The decay is, on the contrary, localized to the region 2500-2800Å, since the difference between the (^{M}L)4p and the (^{M}L)4s states, which determines the wavelength of the fluorescence, is independent of parent term. The decay to the 3d^7 levels falls in a wider wavelength region.

The strongest Fe II lines in the ultraviolet spectrum of RR Tel are the lines at 1776, 1881 and 1884 Å, all from the level (a^{3}F)5p ^{4}D$_{5/2}$. This level is pumped due to a coincidence with the O VI line at 1032 Å (Johansson 1988). The discovery of the fluorescence lines was the first indication of the presence of O VI in the RR Tel system. Later Schmid (1989) resolved the long-standing puzzle of two strong lines unidentified in spectra of many symbiotic stars. He suggested that the O VI lines at 1032 and 1038 Å were Raman scattered by hydrogen atoms. The energy difference between the oxygen lines and H Lyβ was the same as the difference between the scattered lines and Hα. The presence of O VI lines has later been confirmed by direct far-UV observations of the λ1032,1038 lines. The fluorescence lines at 1776 Å might even work as a pumping line itself. This line coincides in wavelength with another Fe II line which connects a low state with a high-excitation state where the latter is seen to have an enhanced population (see Paper I).

The strong fluorescence lines pumped by C IV and O VI are not seen in Eta Carinae, although the H Lyα fluorescence is strong. The reason is the lack of lines or ions responsible for the pumping. The mechanism producing the fluorescent Fe III in Eta Carinae mentioned in the previous section is on the contrary not working in RR Tel, although both H Lyα radiation and Fe^{2+} ions are present.

Chapter 5

A-values for forbidden lines

The most important atomic parameter in many spectroscopic analyses of astrophysical plasmas is the classical oscillator strength (f-value), i.e. the transition probability (the Einstein A-value). This is a measure of the probability that a spontaneous decay occurs from an upper level to a given lower level in a certain time.

One way of determining experimental A-values is to combine a measured radiative lifetime for the upper level with measured branching fractions (BF) for the different decay channels. For a given line the transition probability, A_{ik}, is related to the lifetime, τ_i, and the branching fraction, BF_{ik}, by

$$A_{ik} = BF_{ik}/\tau_i$$

The branching fraction, BF_{ik}, is a measure of the fraction of atoms in level i that decay in the channel ik, i.e. $BF_{ik} = A_{ik}/\sum_k A_{ik}$.

The branching fractions can be obtained by measuring the relative intensities of all lines from an upper level

$$BF_{ik} = \frac{I_{ik}}{\sum_k I_{ik}}.$$

Since the intensities in the equation should reflect the number of photons emitted by the plasma, the observed line intensities have to be calibrated for instrument response and wavelength dependence. For many energy levels studied there are also lines (decay

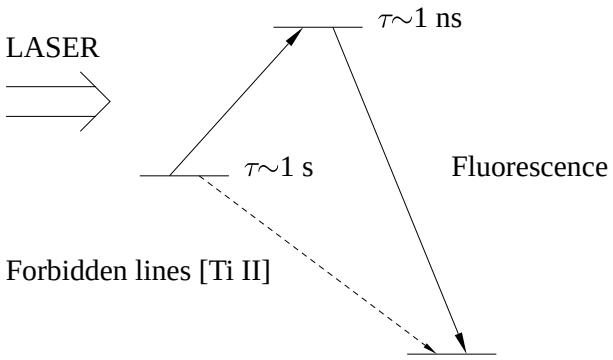

Figure 5.1: Pumping scheme for the Laser Probing Technique (LPT).

channels) that cannot be measured, either because they are too weak or because they fall in an inaccessible wavelength region. The contribution from these lines to the total sum of intensities is usually estimated by theoretical predictions.

To determine absolute A-values for parity forbidden lines the metastable lifetime for the upper level and the relative intensities (BF) of the forbidden lines need to be known. The next section deals with lifetime measurements of metastable levels in complex spectra using a laser probing technique. In the subsequent section the use of forbidden line intensities from astrophysical spectra (the Weigelt blobs in Eta Carinae) to derive branching fractions is considered.

5.1 Lifetime measurements of metastable states

Due to the long lifetime of metastable states, they must be kept in an environment that prevents them from being collisionally deexcited (quenched). This is usually achieved in a vacuum chamber where the probability for collisions with other particles is low. To prevent the ions from hitting the walls they can be stored in either a storage ring or an ion trap. In an ion trap a small number of ions are stored and kept in place by applying magnetic and electric fields.

Storage rings can be used in passive measurements of metastable lifetimes. The ions are accelerated into the ring, most of them being in the ground state but some in excited states. When the metastable ions decay radiatively the spontaneous emission is observed. As time passes the number of ions in the metastable state is reduced, and this is noticed by a decrease in the observed emission. The emitted light is observed in real time in the dominating decay channel, and the lifetime curve is built up (see e.g. Träbert et al. 2003).

To gain statistics the procedure is repeated and the different curves are added. This passive ion storage technique cannot easily be used to measure lifetimes in ions having numerous metastable states. Thus, the lifetime measurements presented in this thesis utilize an active method: the laser probing technique on a stored ion beam, and this is discussed below.

To measure lifetimes of metastable states in complex ions requires a selective technique, where the influence from the other levels can be minimized. The population is distributed among many levels, and the population in each level is thus diluted. The detection efficiency must therefore be increased. At the storage ring in Stockholm, CRYRING (Abrahamsson et al. 1993), a laser probing technique (LPT) applied on a stored ion beam has been successfully used for simpler spectra, such as Ca II and Sr II (Lidberg et al. 1999). This method has proven to be suitable also for complex ions, such as the iron group elements. The probing method meets the requirements of selectivity and high efficiency: one single level can be measured using a tunable laser, and high detection efficiency is obtained by forcing the decay to appear in front of a photo-multiplier.

The method has been developed from the beam-foil and beam-laser spectroscopy methods (see e.g. Andrä et al. 1973). In beam-foil experiments an ion beam passes through a thin carbon foil. After passing the foil the ions are left in excited states which decay spontaneously. The intensity in a decay channel is then measured as a function of the distance from the foil downstream the beam. If the beam energy is known, the distance scale can be converted into a time scale, and the lifetime of the state can be measured. This method is used for states with short lifetimes of the order of a nanosecond. To be able to measure long-lived states, like the metastable states with lifetimes in the second regime, the ions need to travel a very long distance after passing the foil in order to show any change in the emitted light. This is where the storage ring comes in. The ions are left circulating in the ring until a significant decrease in the population can be measured.

Instead of studying the spontaneous decay from the metastable state a laser pulse is used to deplete the state by photoexcitation to a higher level (see Fig. 5.1). The applied laser wavelength should match the transition wavelength to the higher state. In this way most of the ions in the metastable state are transferred to the higher excited state by absorbing the laser light. The higher state chosen should have a short lifetime, of the order of nanoseconds, and thus decay promptly in a fluorescence signal, which is a measure of the population in the metastable state. The method is destructive in the sense that all ions in the state under investigation are depleted and cannot be used for further measurements. After the laser pulse is applied the metastable state is depleted, and a new portion of ions has to be injected and stored in the ring. By applying the laser pulse at different delays after ion injection into the ring, the lifetime curve is built up. Each injection then gives one point on the lifetime curve (see Fig. 5.2).

Since this technique is destructive the experiment requires stable beam conditions. All injections must be equal in terms of the number of ions, and the fraction of metastable

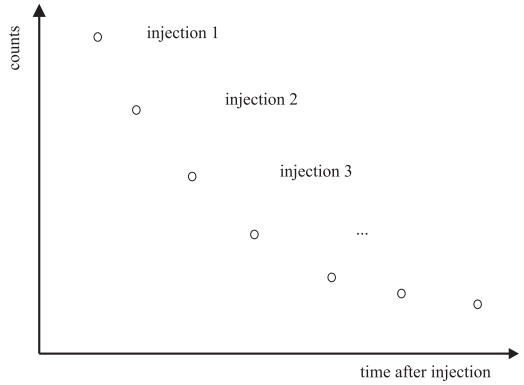

Figure 5.2: Principle for building up the lifetime curve. The points are equally spaced in time.

states may not vary too much. These properties of the ion beam have to be monitored, and, if the conditions are not the same, the various recordings have to be normalized. This is discussed in Sec. 5.2.

The laser beam is merged collinearly with the ion beam in a section of the ring located between two bending magnets, yielding an overlapping distance of a few meters in the measurement section. To prevent the ions from being quenched by the laser at the entrance of this section, the laser wavelength is slightly detuned from the wavelength of the upward transition in Fig 5.1. In front of the PM-tube the ion beam passes through a set of circular electrodes (called DTD, Doppler Tuning Device), which are connected to high voltage. They are set to an electric potential of up to 2 kV. By adding this voltage, the ions are locally accelerated in front of the PM-tube. The faster ions are seeing a Doppler shifted light inside the DTD, and can then be pumped by the detuned laser light. This makes all fluorescence localized to a small region, which is observed by the PM-tube. In addition, by locating the excitation to a point where the electric field has a large gradient the sensitivity to small fluctuations in the laser wavelength or the ion beam energy is minimized. A lens further increases the detection efficiency. Compared to passive monitoring one can reach a factor of 10^4 in gain by using this setup. Because of the relatively low signal achieved for the complex ions with the current setup, the experiment would be impossible to perform without this gain.

5.2 Normalizations and corrections

Besides the raw data recorded for constructing a decay curve for the lifetime measurements other data aimed at normalization and corrections are collected simultaneously. A typical set of curves for such procedures is displayed in Figure 5.3. The problems associated with the destructive technique have been mentioned above, and they are discussed below in more detail followed by a section on corrections associated with collisions with the rest gas.

The disadvantage in using a destructive technique is that the experimental conditions need to be the same during the measurements or that variations should at least be possible to monitor and correct for. The timescale for the duration of each ion injection in the ring is optimally a few times the length of the lifetime measured. Too long a duration time just samples noise when all ions already have decayed and too short a time lacks the late part of the lifetime curve. An estimate of the lifetime to be measured is needed before recording, and it may be obtained from theoretical prediction. If not, a number of test runs need to be performed to optimize the cycle length and the time interval between measured points. Depending on the signal strength, each point on the lifetime curve is typically repeated 10 times to reduce the statistical scatter, and the stability timescale is thus several hours.

The number of ions circulating in the ring is measured for each injection cycle at a fixed time delay after injection. Any possible slow decline of the ion beam current can thus be monitored. The initial fraction of metastable ions per injection is essential since the number of ions left in this state at different times is measured. To monitor the changes in the production of metastable ions fluorescence normalization is performed at fixed intervals, usually every fourth cycle. Then, instead of using a particular point on the lifetime curve, the fluorescence is measured at a fixed delay after injection. If the production rate is the same the fluorescence signal will be constant and only show statistical fluctuations. If a general trend is seen, this can be compensated for. The fluorescence normalization is basically the same as measuring the same point on the lifetime curve over and over again.

The fluorescence signal is detected using a photomultiplier (PM) tube. This has a large spectral sensitivity region, and the effect from the laser light needs to be filtered away. A colored glass filter is used for this purpose and chosen to transmit the fluorescence light and block the laser light at longer wavelength. The background due to scattered light is of the order of 10 s^{-1} which adds a few counts per channel. The filter typically lets almost all light through in the fluorescence channels but only fractions of a percent in the laser light region.

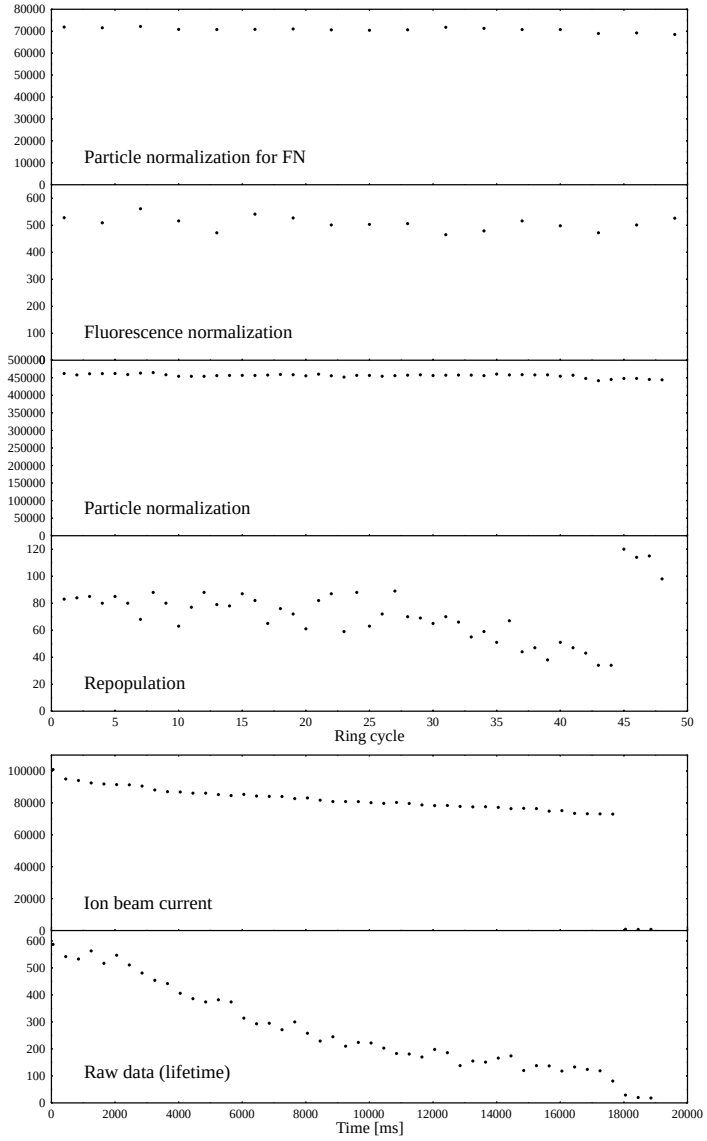

Figure 5.3: A typical set of curves recorded during a lifetime measurement. (From measurements of the level $b^4P_{1/2}$ in Ti II.)

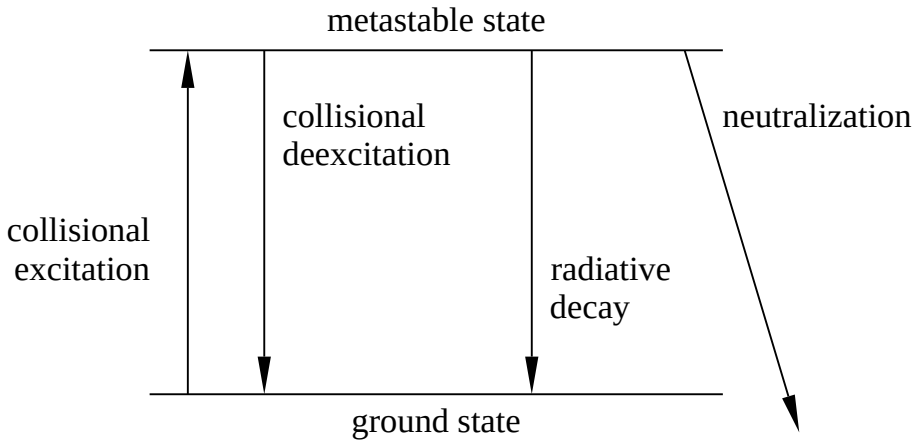

Figure 5.4: Processes affecting the population in the metastable level. The radiative decay is the quantity of interest and other effects need to be minimized or corrected for.

Repopulation

The atomic parameter we want to measure is the radiative lifetime, which would be obtained directly if the decreasing number of ions in the metastable state was only due to the radiative decay. In reality, collisions with the rest gas in the storage ring also affect the population. Collisional deexcitation depletes the states without any photon being emitted. This effect is observed as a change in the measured lifetime when changing the pressure in the ring, since the collisional deexcitation is pressure dependent. The reverse process, collisional excitation, is also observed. Only a small fraction, of the order of 1%, of the stored ions are in the excited state; the majority are in the ground state. When they collide with the rest gas the atom might end up in the metastable level studied. When this process is significant the lifetime appears longer and might deviate from a single exponential decay. Significant repopulation was first observed in an experiment on Ca^+ (Mannervik et al. 1997). The lifetime decay curve did not approach zero but rather a constant non-zero level. This is interpreted as an equilibrium between the radiative and collisional decay on one hand and the collisional excitation on the other. To correct for this effect a separate 'repopulation curve' is recorded separately in the following way in a separate measurement.

Immediately after injection a laser pulse is applied, long enough to empty the metastable state completely. The laser is then blocked and the ion beam interacts with the rest gas. A second laser pulse is applied to probe the number of ions in the metastable states, which are all created via collisional excitation. As for the lifetime curve, the delay after injection

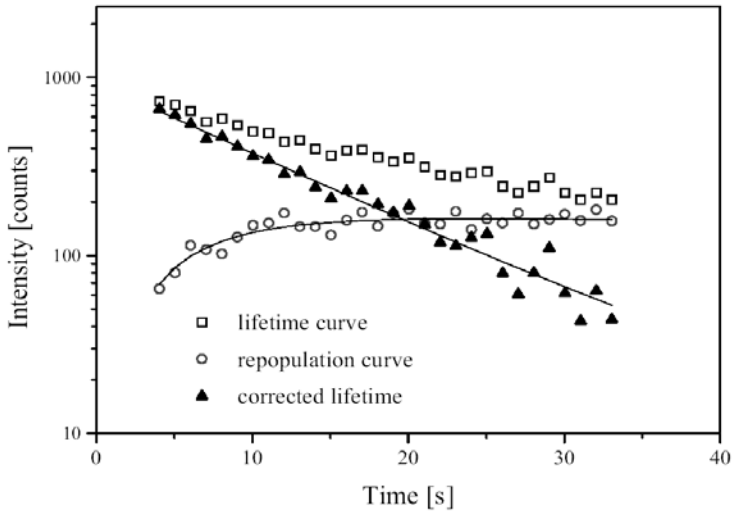

Figure 5.5: The effect of repopulation for $b^4P_{5/2}$ in Ti II (Paper VIII).

is varied for this second laser pulse. The collisional excitation of the metastable state (the repopulation) can then be monitored. This curve is subtracted from the raw lifetime curve to get the corrected decay curve. By doing this subtraction, the ions produced by collisions are removed and left are only the initial ions produced in the ion source. The repopulation effect is particularly significant for some states, and a typical example is shown in Figure 5.5 for $b^4P_{5/2}$ in TiII.

In the most recent experiments a new technique for obtaining the repopulation curve has been developed. The repopulation curve is then obtained simultaneously with the lifetime curve. The repopulation pulse is applied at a fixed time delay after injection, right before the beam is dumped. The moving probe pulse for the lifetime measurements then works as an outpumping pulse. The time delay between the two pulses is varied as the pulse for the lifetime measurements is stepped in time. The raw repopulation curve in Fig. 5.3 is obtained using this new technique. After correction and normalization the repopulation curve has the same shape as a curve obtained in a separate measurement, as shown in Fig. 5.5. The advantages are a gain in time, since no separate measurement is needed, and also a more reliable normalization. The disadvantage is that the repopulation is measured at the end of the injection cycle where the number of ions is less. This new technique is discussed in more detail by Ellmann (2003).

Collisional quenching

Collisions with the rest gas are working in the opposite direction as well, decreasing the number of metastables. This is observed as a shortening of the lifetime. The effect of collisional deexcitation is studied by changing the pressure in the ring. Despite the low base pressure (P<10^{-11} mbar) this effect is not negligible. It provides an extra decay channel, and long lifetimes are affected more than short ones. By measuring the apparent lifetime of the state for a series of pressures in the ring and extrapolating to zero pressure one can correct for the collisional quenching. This is done in a so called Stern-Vollmer plot. The measured decay rate, which includes both the radiative and collisional decay rates, is plotted against the relative pressure, as shown in Fig. 3 in Paper III.

The pressure cannot be changed homogeneously throughout the whole ring. Instead, one NEG-pump (Non Evaporate Getter) is heated by changing a variable voltage. The pressure is then locally raised, resulting in an average increase of the pressure by one order of magnitude. The pressure cannot be measured using the vacuum gauges, but instead the ion beam lifetime is used as a probe since neutralization in collisions with the rest gas is assumed to be the main reason for the ion beam decay. After one of the bending magnets an NaF-detector measures the number of neutralized particles, which represents the relative beam intensity. The lifetime of the ion beam is used as a measure of the relative pressure in the Stern-Vollmer plot.

5.3 Limitations

In Paper VIII we present what we believe is the longest radiative lifetime measured so far in a storage ring, viz. 28 s for the $b^4P_{5/2}$ level in Ti II. This is close to the upper limit for the present technique. For long lifetimes the competing deexcitation processes, collisional quenching and neutralization of the ion beam, become more important and the corrections, and thereby the error, increase. The lifetime of the ion beam is of the order of 1 minute for base pressure and smaller for increased pressure. To get a reliable correction for the collisional quenching it is necessary to record a good lifetime curve for both base and high pressure.

In addition to the lifetime of the measured state, the atomic structure may also limit the number of elements that can be studied by this technique. During the measurements the ions are transferred to a higher state of opposite parity, which decays promptly and the fluorescence be observed. There are thus requirements on the pumping channel, the laser frequency and the fluorescence channels that must be fulfilled to make measurements of the lifetime possible:

- **Pumping channel:** The pumping channel needs to be strong (i.e. have a large transition probability) and have a wavelength accessible to the laser used. In the present experiments we have used a cw dye laser working in two separate regions around 650 and 400 nm, respectively. If the metastable level to be measured has a very low excitation energy, the energy difference to the next level with opposite parity might be large (see e.g. Fig. 5.1). The wavelength needed to match this energy difference requires a tunable laser that operates in the UV-region. For example, forbidden lines from the metastable Ni II levels at $3d^8(^3F)4s\ ^2F$ are often used for diagnostics of astrophysical plasmas. In order to measure the lifetime, tunable cw laser light at 250 nm is needed to reach the lowest level of odd parity.
- **Fluorescence channels:** The highly excited, laser pumped levels decay promptly in more than one fluorescence channel, and one of them is obviously the pumped channel itself. The branching fraction for that transition should be significant but not dominate the decay, since that will result in a fluorescence having the same wavelength as the laser light. All fluorescence signals would be blocked by the PM-filter, which prevents the laser light from being observed. Fluorescence channels with similar wavelengths as the pumping channel will also be blocked since the filters are not narrow enough to separate out light close in wavelength.
- **Wavelength coincidences:** Ions with complex spectra, such as Fe II and Ti II, have many spectral lines. One has to be aware of blending lines that could affect the measurements. These include lines that might deplete the measured state outside the view of the PM-tube or lines from other metastable levels coinciding with the pumping wavelength and thereby adding fluorescence also from other levels to the detected signal.

5.4 Lifetime results

Within the FERRUM project (Johansson et al. 2002) experimental lifetimes for four metastable levels in Fe II and two in Ti II in the range 0.33 to 28 s have been published (see Table 5.1). Three more Ti II levels have been measured recently and the data are now being analyzed.

5.5 Branching fractions for forbidden lines

The measurements of intensities of forbidden lines are difficult to perform using ordinary laboratory sources, such as a hollow cathode, since the metastable levels are quenched if they are not stored in a low pressure environment. One possibility is to keep the ions in a storage ring, monitor the decay in the different lines and compare the line ratios. In order

Table 5.1: Measured metastable lifetimes within the FERRUM project.

Ion	Level	Lifetime (s)
FeII	$3d^5 4s^2\ a^6S_{5/2}$	0.23(3)
	$(^3G)4s\ a^4G_{9/2}$	0.65(2)
	$(^3H)4s\ b^2H_{11/2}$	3.8(3)
	$(^3D)4s\ b^4D_{7/2}$	0.53(3)
TiII	$3d^3\ a^4P_{5/2}$	28(10)
	$3d4s^2\ c^2D_{3/2}$	0.33(20)

to do this for a complex ion one needs to separate not only the different decays from the level measured but also the lines from all other metastable states decaying simultaneously. A high spectral resolution is thus needed. Also, since the decay is slow the count rate for forbidden lines is low, and if a passive technique is used the decay is not spatially located but spread all over the ring. By using the laser probing technique in the lifetime measurements discussed in the previous section a factor of 10^4 is gained compared to passive monitoring. For complex ions passive monitoring of the decay has a low signal and measurements of branching fractions would be very difficult.

To get a detectable signal in a forbidden line the number of metastable ions, in a low density plasma, has to be sufficiently large. This requires a large volume. These conditions exist in astrophysical plasmas, and the intensity of forbidden lines in the integrated light of such sources can be observed and used for measuring branching ratios. But, other observational problems arise when studying astrophysical plasma sources. Neither the chemical composition nor the physical properties of the plasma gas can be controlled. In addition, the light emitted from the plasma may be affected by gas and dust along the line of sight, and the observed line ratios often differ from the true line ratios due to scattering. The blue light is scattered more efficiently and therefore the light appears reddened. This has to be compensated for when deriving the branching fractions from astrophysical emission line spectra.

The effect from reddening by the interstellar medium (ISM) has been studied for many stars at different distances and in different directions. The reddening curve, i.e. the effect of scattering as a function of wavelength, is observed to have a similar shape for the different stars, but the amount of reddening is on the contrary not the same for individual stars but depends on the amount of material in the line of sight.

We have used the Weigelt blobs, which are low-density gas condensations close to the massive star Eta Carinae, to derive the relative intensities for forbidden [Fe II] lines. The spectrum shows strong emission lines and is rich in Fe II and [Fe II] (Zethson 2001). The object has been observed with the Hubble Space Telescope (HST) and spectra recorded

with the Space Telescope Imaging Spectrograph (STIS), and these spectra offer a good spatial resolution, which minimizes the influence of lines from other spatial regions. The spectra have a spectral resolution that is good enough to separate out the different lines and still offer a good signal-to-noise ratio (S/N) (see Ch. 3). The effect from blending emission features from the same plasma or from other locations along the line of sight can not be avoided but can, to some extent, be corrected for.

The [Fe II] lines from the blobs are affected by scattering from other regions of Eta Carinae as well as from the interstellar medium. The common way of determining the amount of reddening is by studying the branching ratio of two lines (from the same upper level) and compare with the theoretical branching ratio (the ratio of the corresponding A-values). By applying this branching ratio to a standard reddening curve, the amount of reddening can be derived. But, the A-values are what we want to measure, so in order to get around this we use all possible [Fe II] lines from the blobs and use the theoretical transition probabilities to determine the reddening, assuming a standard reddening curve (Osterbrock 1989). To be used as a measurement of the reddening the lines from a certain level must fulfill a number of criteria:

- The emission lines from the upper level must have a span in wavelength so that they are affected by scattering by different amounts.
- The lines are ideally unblended and strong enough to be measured accurately.

We found 14 [Fe II] lines that were possible to use for the derivation of the amount of reddening. For each line pair a reddening coefficient C was calculated according to

$$\frac{I_{\lambda_1}}{I_{\lambda_2}} = \frac{I_{\lambda_1,0}}{I_{\lambda_2,0}} \cdot e^{-C[f(\lambda_1)-f(\lambda_2)]}$$

using the average reddening curve from Osterbrock (1989,Table 7.2). This reddening curve is based on the assumption that the amount of scattering as a function of wavelength has the same shape, $f(\lambda)$, everywhere but with different amount of extinction, C, depending on the material along the line of sight.

These line ratios resulted in a reddening with an average value of C=1.6, with a standard error of 0.4. Observed inconsistencies for the different line pairs are due to line blending, uncertainties in line flux measurements and deviations in the theoretical A-values. In addition, the light passes through parts of the nebula as well, and this might affect the line ratios in a way that is not described by the average reddening curve. This will cause differences in the C-values derived from different line pairs, depending on their wavelength.

From $b^4D_{7/2}$ the different lines appear between 3200 and 5600Å, which means that the reddening is significant and the observed branching fractions had to be corrected.

For $a^4G_{9/2}$ and $a^6S_{5/2}$, the major part of the emission falls in a narrow wavelength region, and line ratios are thus not sensitive to reddening. The final line ratios for these levels were corrected for reddening but the overall effect was less than 1%.

5.6 A-values

In total, we derived experimental A-values for 13 forbidden [Fe II] lines from 3 levels in Fe II, namely $(^3G)4s\ a^4G_{9/2}$, $3d^54s^2\ a^6S_{5/2}$ and $(^3D)4s\ b^4D_{7/2}$. The results for the different lines are given in Table 5 in Paper VII. In addition, we combined the theoretical branching fractions (Quinet et al. 1996) with our measured lifetime for the $(^3H)4s\ b^2H_{11/2}$ level to obtain semi-experimental A-values for forbidden lines from this level.

The parameters used in the derivation of A-values are treated as independent variables, and we derived the total uncertainty in the experimental A-values using the Gauss approximation formula for independent variables (see Appendix B for a detailed discussion). The values are not independent but this was done in order to get an estimate of the uncertainties. This resulted in uncertainties for the astrophysical A-values in the range 10 to 25%. The larger uncertainties are for the $b^4D_{7/2}$ level, and the largest contribution comes from the reddening correction.

In conclusion, the measurements at CRYRING of lifetimes for metastable states of complex spectra are the first experimental tests of the theoretical data used for diagnostics of astrophysical plasmas. Our measurements show that the theoretical values are, in general, accurate enough for this purpose except for lines originating from energy levels, which we know are strongly mixed with other states.

Chapter 6

The papers

The papers included in this thesis can be grouped into three cathegories:

Papers I and II deal with identification of fluorescence lines, pumping lines and forbidden lines in satellite spectra of RR Tel and the environments of Eta Carinae.

Papers III, IV and V present and consider the detection of forbidden [Sr II] lines in HST spectra of a particular region in the Eta Carinae nebula. Plasma diagnostics and line identification in subsequent observations of this region are also included.

Papers VI, VII and VIII describe lifetime measurements of metastable levels in Fe II and Ti II. This work has been performed at CRYRING (Stockholm, Sweden) in collaboration with the Atomic Physics group at Stockholm University, and it was initiated by the need for atomic data in the analysis of spectra from the strontium filament of Eta Carinae mentioned above. The spectrum of the Weigelt blobs in Eta Carinae is used to derive branching fractions to determine absolute A-values for forbidden lines in Fe II.

The papers are discussed individually below, and my contribution to each paper is specified.

Paper I: Ultraviolet fluorescence lines of Fe II observed in satellite spectra of the symbiotic star RR Telescopii

Hartman, H., Johansson, S.
A&A **359**, 627 (2000)

The ultraviolet spectrum of the symbiotic star RR Telescopii is dominated by lines from light elements in a large number of ionization stages, together with numerous lines from specific highly excited levels in Fe II. The latter lines are explained as fluorescence lines. Due to wavelength coincidences between strong emission lines and transitions from low states in Fe II, the high excitation states are populated. We list the fluorescence lines observed and the pumped levels along with the line and element responsible for the pumping.

I did the majority of the work and was reponsible for preparation of the manuscript.

Paper II: New forbidden and fluorescent Fe III lines identified in HST spectra of η Carinae

Johansson, S., Zethson, T., **Hartman, H.**, Ekberg, J.O., Ishibashi, K., Davidson, K., Gull, T.
A&A **361**, 977 (2000)

In this paper we report new forbidden lines along with theortical transition probability data for the $3d^6$ a^5D- $3d^54s$ a^5S transitions in Fe III. The [Fe III] lines are observed in RR Tel and Eta Carinae. In addition, a wavelength coincidence with H Lyα and a level mixing open a fluorescence channel in Fe III, which results in an enhancement of the 1914 Å line (UV34) in Eta Carinae. This enhancement is not observed for RR Tel, although both H Lyα pumping of Fe II and forbidden lines from [Fe III] are observed.

My contribution to this paper is the analysis concerning RR Tel. I did not perform any atomic calculations.

Paper III: Sr II and [Sr II] Emission in the Ejecta of Eta Carinae

Zethson, T., Gull, T., **Hartman H.**, Johansson, S., Davidson, K., Ishibashi, K.
AJ **122**, 322 (2001)

During a HST/STIS mapping project of the Eta Carinae nebula, a region with forbidden [Sr II] emission was observed. This paper reports the first identification of [Sr II] in an astrophysical spectrum and about 20 other emission lines in the wavelength region 6490-7050Å.

I participated in the line identification work.

Paper IV: Excitation of Sr II lines in Eta Carinae

Bautista, M. A., Gull, T.R., Ishibashi, K., **Hartman H.**, Davidson, K.
MNRAS **331**, 875 (2002)

In paper IV we perform a modelling of the Sr^+ ion trying to reveal the excitation process behind the strontium lines in Eta Carinae and any possible overabundance of strontium. The line strengths of the Sr II and [Sr II] lines can be explained with a plasma electron density of $10^7 cm^{-3}$ and a weak radiation field.

I contributed to the spectral analysis and participated in the discussion. I did not perform any modelling of the plasma or ions.

Paper V: Identification of Emission Lines in the Low-Ionization Strontium Filament Near Eta Carinae

Hartman, H., Gull, T.R., Johansson, S., Smith, N., HST Eta Carinae Treasury Project Team
Submitted to A&A

Spectral HST/STIS observations in the wavelength range 1635-10140 Å of the strontium filament revealed 600 emission lines, which are reported in Paper V. The long slit mode of STIS is used to distinguish the emission of the filament from the emission from other plasmas along the line of sight. Due to a number of different slit orientations, a better understanding of the spatial extent of the plasma is retrieved.

I performed the line identifications and was responsible for preparation of the manuscript. I did not take part in the reduction of the data.

Paper VI: Lifetime Measurements of Metastable States in Fe^+

Rostohar, D., Derkatch, A., **Hartman, H.**, Johansson, S., Lundberg, H., Mannervik, S., Norlin, L.-O., Royen, P., Schmitt, A.
Phys. Rev. Lett. **86**, 1466 (2001)

Paper VI reports on the first experimental lifetime measurements of metastable ions in complex spectra using a laser probing technique. We measured the lifetimes of the metastable levels $a^6S_{5/2}$ and $b^4D_{7/2}$ in Fe II. These lines are strong in the emission line spectrum of the Weigelt blobs in Eta Carinae.

I participated in the experiment and was responsible for the planning as regards the energy levels and spectral lines involved. I took part in the dicussion of the development of the expermintal technique but did not perform any data reduction.

Paper VII: The FERRUM Project: Experimental transition probabilities of [Fe II] and astrophysical applications

Hartman, H., Derkatch, A., Donnelly, M. P., Gull, T., Hibbert,A. , Johansson, S., Lundberg, H., Mannervik, H., Norlin, L.-O., Rostohar, D., Royen, P., Schef, P.
A&A **397**, 1143 (2003)

One of the atomic parameters needed for plasma diagnostics is the transition probability (the A-value). One way of deriving this is to combine the radiative lifetime of the upper level with the branching fractions (BF) of all decay channels. The lifetime is measured using laser probing on a stored ion beam. Since the metastable states are easily quenched in most laboratory sources we used the plasma around the star Eta Carinae to derive the BF's for the forbidden [Fe II] lines from the levels $a^6S_{5/2}$, $a^4G_{9/2}$ and $b^4D_{7/2}$. The lines from $b^4D_{7/2}$ had to be corrected for reddening, which affects the line intensities differently in different wavelength regions. In addition, semiempirical A-values are reported for $b^2H_{11/2}$. The experimental A-values are compared to previous and recent calculations.

I performed several measurements in the experiment, and decided what levels to measure and lines to use. I derived the astrophysical branching fractions. I did not take part in the data reduction or the atomic calculations.

Paper VIII: The FERRUM project: an extremely long radiative lifetime in Ti II measured in an ion storage ring

Hartman, H., Rostohar, D., Derkatch, A., Lundin, P., Schef, P., Johansson, S., Lundberg, H., Mannervik, S., Norlin, L.-O., Royen, P.
A&A **397**, 1143 (2003)

In Paper V we reported on the identification of 600 emission lines from the strontium filament. The majority of these lines come from Ti II and [Ti II], which are observed to be very strong. As is discussed in the introduction of this thesis, the forbidden [Ti II] lines can be used for astrophysical plasma diagnostics. Since they are superiour in number compared to [Sr II] more information can be obtained from [Ti II].
In Paper VIII we report on the long lifetime of $b^4P_{5/2}$ in [Ti II]. The lifetime of 28 s is approaching the upper limit of what is possible to measure using the present technique.

I was responsible for the spectroscopic planning of the experiment, participated in the experiment and the discussion and development of the technique used. I did not perform any data reduction.

Appendix A

Identified fluorescence mechanisms

A number of fluorescence mechanisms have been identified since the first explanation by Bowen (1928). These are present in different plasmas, such as planetary nebulae, symbiotic stars and atmospheres of cool stars, showing emission lines. Below is a compilation of known fluorescence processes.

Ion	Pumped level	Energy (cm^{-1})	Pumping line	Ref
O I	$2p^3(^4S)3d\ ^3D$	97488	H Lyβ	B47
S I (UV9)	$3p^34s\ ^3P_1$	77150	O I 1304	BJ80
S I (UV9)	$3p^34s\ ^3P_2$	77181	O I 1304	BJ80
Ti I	v^1P_1	42927	Mg II 2802	T37
V I	$u^4D_{7/2}$	35379	Mg I 2852	T37
Cr I	s^5F_4	50210	Fe II 2373	T37
Cr II	$4s4p\ x^6D_{1/2}$	93968	H Lyα	ZHJ01
Cr II	$5p\ ^4P_{5/2}$	93974	H Lyα	ZHJ01
Cr II	$5p\ ^6P_{3/2}$	94002	H Lyα	ZHJ01
Cr II	$4s4p\ x^6D_{3/2}$	94098	H Lyα	ZHJ01
Cr II	$5p\ ^6P_{5/2}$	94144	H Lyα	ZHJ01
Cr II	$5p\ ^4F_{3/2}$	94256	H Lyα	ZHJ01
Cr II	$4s4p\ x^6D_{5/2}$	94265	H Lyα	ZHJ01
Cr II	$5p\ ^6P_{7/2}$	94363	H Lyα	ZHJ01
Cr II	$5p\ ^4F_{5/2}$	94365	H Lyα	ZHJ01
Cr II	$4s4p\ x^6D_{7/2}$	94452	H Lyα	ZHJ01

Ion	Pumped level	Energy (cm^{-1})	Pumping line	Ref
Cr II	$5p\ ^4F_{7/2}$	94522	H Lyα	ZHJ01
Cr II	$4s4p\ x^6D_{9/2}$	94656	H Lyα	ZHJ01
Cr II	$5p\ ^4F_{9/2}$	94749	H Lyα	JC88
Mn I	$y^6P_{7/2}$	35769	Mg II 2795	C70
Mn II	$3d^5(^6S)4f\ ^5F_1$	98461	Si II 1197.57	JWG95
Mn II	$3d^5(^6S)4f\ ^5F_2$	98462	Si II 1196.72	JWG95
Mn II	$3d^5(^6S)4f\ ^5F_3$	98463	Si II 1195.00	JWG95
Mn II	$3d^5(^6S)4f\ ^5F_4$	98464	Si II 1192.31	JWG95
Mn II	$3d^5(^6S)4f\ ^5F_5$	98465	Si II 1190.41	JWG95
Fe I	z^3G_4	35767	Mg II 2795	T37
Fe I	z^3G_3	36079	Mg II 2802	T37
Fe I	y^3F_3	37162	Ca II 3968	C70
Fe I	y^3D_2	38678	Hξ	C70
Fe I	y^3D_1	38995	Fe II 2611	WC90
Fe I	x^5F_1	41130	Fe II 2484	T37
Fe I	x^5P_3	42532	Fe II 2373	T37
Fe I	x^5P_2	42859	Fe II 2382	T37
Fe I	y^5G_3	43137	Mg II 2795	T37
Fe I	y^5G_2	43210	Mg I 2852	T37
Fe I	w^5D_4	43499	Mg II 2795	T37
Fe I	v^5D_3	44166	Fe II 2714	WC90
Fe I	w^5D_2	44183	Fe II 2761	T37
Fe I	x^5G_5	45726	Fe II 2607	T37
Fe I	w^3P_1	50043	Hξ, H16	C70
Fe II	$(^3H)4p\ z^4G_{9/2}$	60807	Si III] 1892	HJ00
Fe II	$(^3H)4p\ z^4G_{5/2}$	61041	[Fe IV] 2835	HJ00
Fe II	$z^4I_{13/2}$	61527	Fe II UV33, 207, 63	CP88
Fe II	$(^3H)4p\ z^2G_{9/2}$	62083	O III] 1661	HJ00
Fe II	$y^4G_{5/2}$	64087	Fe II 2628/2359	CP88
Fe II	$(^3G)4p\ x^4G_{7/2}$	65931	[Ne V] 1575	HJ00
Fe II	$x^4G_{5/2}$	66078	Fe II 2599	CP88
Fe II	$(^3G)4p\ y^4H_{11/2}$	66463	C IV 1548	J83
Fe II	$(^3G)4p\ x^4F_{5/2}$	66522	Si III] 1892	HJ00
Fe II	$(a^1G)4p\ x^2H_{9/2}$	72130	<Fe II> 1776	HJ00
Fe II	$(a^1D)4p\ w^2D_{3/2}$	78487	C IV 1548	HJ00
Fe II	$(b^3F)4p\ ^4G_{9/2}$	90042	H Lyα	JJ84
Fe II	$(^5D)5p\ ^6F_{9/2}$	90067	H Lyα	JJ84
Fe II	$(^5D)5p\ ^6F_{7/2}$	90300	H Lyα	MJC99

Ion	Pumped level	Energy (cm^{-1})	Pumping line	Ref
Fe II	$(^5D)5p\ ^4F_{9/2}$	90386	H Lyα	MJC99
Fe II	$(^5D)5p\ ^4D_{7/2}$	90397	H Lyα	MJC99
Fe II	$(b^3P)4p\ ^4S_{3/2}$	90629	H Lyα	JJ84
Fe II	$(^5D)5p\ ^4D_{5/2}$	90638	H Lyα	JJ84
Fe II	$(^5D)5p\ ^4F_{7/2}$	90780	H Lyα	JJ84
Fe II	$(b^3P)4p\ ^4P_{1/2}$	90839	H Lyα	JJ84
Fe II	$(b^3P)4p\ ^4P_{3/2}$	90898	H Lyα	JJ84
Fe II	$(^5D)5p\ ^4P_{5/2}$	90901	H Lyα	JJ84
Fe II	$(^5D)5p\ ^4D_{3/2}$	91048	H Lyα	JJ84
Fe II	$(^5D)5p\ ^4F_{5/2}$	91070	H Lyα	JJ84
Fe II	$(^5D)5p\ ^4D_{1/2}$	91199	H Lyα	JJ84
Fe II	$(^5D)5p\ ^4F_{3/2}$	91208	H Lyα	JJ84
Fe II	$(^4G)4s4p(^3P)\ x^4H_{11/2}$	92166	He II 1084	JH98
Fe II	$(b^3F)4p\ u^2G_{9/2}$	92171	He II 1084	HJ00
Fe II	$(b^3F)4p\ u^4F_{3/2}$	93328	N IV] 1487	HJ00
Fe II	$(^4P)4s4p\ ^4D_{3/2}$	95858	H Lyα	CP88
Fe II	$(^1G)4p\ ^2H_{11/2}$	98278	H Lyα	MJC99
Fe II	$(^4P)4s4p(^xP)\ ^2S_{1/2}$	103967	H Lyα	MJC99
Fe II	$(^2D)4s4p(^3P)\ ^4F_{7/2}$	104907	H Lyα/ O V 1218	JC88
Fe II	$(^2F)4s4p(^xP)\ ^4G_{9/2}$	107674	H Lyα	MJC99
Fe II	$(^2F)4s4p(^3P)\ ^4G_{11/2}$	107720	H Lyα	JJ84
Fe II	$(^4F)4s4p(^xP)\ ^6D_{5/2}$	108130	H Lyα	MJC99
Fe II	$(^2F)4s4p(^xP)\ ^4F_{9/2}$	108217	H Lyα	MJC99
Fe II	$(^4F)4s4p(^3P)\ ^6D_{7/2}$	108239	H Lyα	MJC99
Fe II	$(^4G)4s4p(^1P)\ ^4H_{9/2}$	108868	Ne V 1146/Si III 1207	JH98
Fe II	$(a^3F)5p\ ^4D_{5/2}$	110568	O VI 1032	J88
Fe III	$3d^5(^6S)4p\ z^7P_3$	82333	H Lyα	JZH00
Zr I	x^1G_4		Mg II 2795	B47
In I	$d\ ^2S_{1/2}$		Hγ	T37

B47 = Bowen (1947)
BFJ81 = Brown et al. (1981)
BJ80 = Brown & Jordan (1980)
C70 = Cowley (1970)
CP88 = Carpenter et al. (1988)
HJ00 = Hartman & Johansson (2000)
HLW77= Haisch et al. (1977)
J83 = Johansson (1983)
J88 = Johansson (1988)
JC88 = Johansson & Carpenter (1988)
JH98 = Jordan & Harper (1998)
JJ84 = Johansson & Jordan (1984)
JWG95 = Johansson et al. (1995)
JZH00 = Johansson et al. (2000)
MJC99 = McMurry et al. (1999)
T37 = Thackeray (1937)
WC90 = Wahlgren & Carpenter (1990)
ZHJ01 = Zethson et al. (2001)

Appendix B

Uncertainties of astrophysical A-values

The uncertainties for the astrophysical A-values are derived using the Gauss approximation formula of independent variables. Sikström et al. (2002) applied this formula to derive consistent error bars for oscillator strengths for E1 transitions where the branching fractions (BF's) are measured using a Fourier Transform Spectrometer. We follow the same recipe when deriving the BF's from an astrophysical source, but we use a different set of sources for uncertainties. For example we need to treat the uncertainties introduced by the corrections for the reddening.

We realize that all uncertainties are not independent and they can thus not strictly be treated using the equation below since it assumes independent variables. For example, each line used to derive the reddening is used in more than one ratio, which clearly does not give independent results.

The expression is used to get an estimate of the quality of the result rather than to derive strict error bars. Below the different errors are discussed in more detail for the different levels.

We have modified the expression used by Sikström et al. (2002) used for the relative uncertainties for the A-values as follows:

$$\begin{aligned}\left(\frac{u_c(A_k)}{A_k}\right)^2 &= (1-2(BF_k))\left(\frac{u_c(I_k)}{I_k}\right)^2 \\ &+ \sum_{j=1}^{n}(BF_j)^2\left(\left(\frac{u_c(I'_j)}{I'_j}\right)^2+\left(\frac{u_c(c_j)}{c_j}\right)^2+\left(\frac{u_c(I_{red})}{I_{red}}\right)^2\right) \\ &+ (BF_{res})^2\left(\frac{u_c(I_{res})}{I_{res}}\right)^2 \\ &+ \left(\frac{u_c(\tau)}{\tau}\right)^2\end{aligned}$$

The first term includes the uncertainty in the measurement of the intensity for the current line. Since the relative intensity is the interesting parameter, the uncertainty in the intensities of the other lines from the same upper level also affect the BF. These are included in the second term. The third term includes the uncertainty of the residual and the last term the uncertainty of the measured lifetime. The parameters in the above expression are:

- BF_k : branching fraction for the current line
- $u_c(I_k)$: Uncertainty in the intensity measurement of line k. We have used 3 different observations from three different dates to check the consistancy.
- $u_c(c_j)$: Uncertainty in the intensity calibration. The intensity calibration for the different lines is treated independent. The uncertainty for close lines is smaller than for distant lines. An uncertainty of 5% in the relative intensity is assumed.
- $u_c(I_{red})$: Uncertainty in the effect from reddening. Different values for the reddening constant C are applied and the expected intensities are compared. This term applies only for the $\mathrm{b}^4\mathrm{D}_{7/2}$ level.
- $u_c(I_{res})$: Uncertainty in the calculated residual, i.e. the lines not seen. We have used the calculations from Quinet et al. (1996) to derive the residuals.
- $u_c(\tau)$: Uncertainty in the experimental lifetime (for a detailed dicussion, see Paper VI & VII). The values and uncertainties for the different levels are $\mathrm{a}^6\mathrm{S}_{5/2} = 230(30)$ ms, $\mathrm{a}^4\mathrm{G}_{9/2} = 650(20)$ ms and $\mathrm{b}^4\mathrm{D}_{7/2} = 530(30)$ ms.

Comments for the different levels are given below.

a$^6S_{5/2}$

All lines are strong and unblended, except for the λ4359 line. The uncertainty of the intensity measurements are estimated to 5% for the unblended lines and 15% for the λ4359 line. The residual for this level is 0.1%.

a$^4G_{9/2}$

One of the lines is blended by an FeII line ($a^2D_{5/2}$-$z^4D_{7/2}$) which contributes with 20% to the total intensity of this line. The contribution is determined by comparing other lines from the upper level $z^4D_{7/2}$ and an error of 10% of the total intensity (i.e. 50% of the contributing intensity from this transition) is assumed.

b$^4D_{7/2}$

For the level $b^4D_{7/2}$ the correction for the reddeningis an additional source of uncertainty. This is determined by changing the value for the reddening constant C and study the corresponding change in the A-values. The uncertainty introduced from the reddening correction spans from 5% to 22%, with the higher values for the yellow lines. This uncertainty is dominating.

Populärvetenskaplig sammanfattning

Mycket av dagens forskning inom astrofysik handlar på ett eller annat sätt om att förstå hur universum i allmänhet och vår galax i synnerhet fungerar. Var och hur har de grundämnen bildats som finns i stjärnor, planeter, gasmoln, på jorden och i våra kroppar? Det dominerande, och framgångsrika, sättet att ta reda på hur avlägsna astronomiska objekt ser ut och är uppbyggda är att studera ljuset som de sänder ut.

Atomer från alla sorters grundämnen sänder ut ett karakteristiskt ljus. Ljuset som ett ämne sänder ut ändras dessutom beroende på förhållandena i gasen där atomerna befinner sig; olika temperatur, densitet och strålningsfält i plasmat gör att olika våglängder favoriseras. Att analysera ljuset från en stjärna eller ett gasmoln kan således ge kunskap om förhållanden där ljuset skickas ut. Med hjälp av en spektrograf delas ljuset upp i de ingående färgerna, ett spektrum. Det innehåller det blandade ljuset från alla atomer i gasmolnet. Motsvarande spektrum från ett laboratorieplasma innehåller bara linjer från de ämnen som finns i ljuskällan. Om spektralanalys av ett grundämne i laboratoriet liknas vid att studera ett ämnes fingeravtryck kan spektralanalys av ett astronomiskt objekt liknas vid att studera fingeravtrycken på ett dörrhandtag. Laboratoriespektrerna tjänar då som referens. Genom att sortera ut enskilda avtryck från handtaget kan man inte bara se vem som passerat, utan också hur många gånger och kanske hur snabbt.

Elektronen kan bara röra sig i speciella banor runt atomen. Dessa banor är olika för olika ämnen. Atomens karakteristiska ljus uppkommer när elektronen byter bana och skickar ut den extra energin som ljus av en speciell färg. Det är dessa ljusblixtar, fotoner, som observeras i spektrumet. Varje övergång motsvarar en specifik färg, en våglängd. Genom att jämföra de observerade våglängderna från stjärnan med laboratorievåglängder kan grundämnena i stjärnan identifieras. Hur länge elektronen stannar i en yttre bana, ett exciterat tillstånd, innan den skickar ut en foton är också intressant. Med hjälp av den tiden, det exciterade tillståndets livstid, kan man ta reda på vissa förhållanden i gasen, såsom täthet och temperatur.

Att mäta livstiden för en energinivå, dvs den förväntade tid den befinner sig här innan den faller tillbaka, kan jämföras med att studera antalet bitar i en skål godis. I början minskar antalet fort men det äts allt långsammare när antalet sjunker. Likadant är det med en grupp atomer som befinner sig i ett exciterat tillstånd. De flesta hoppar ner snabbt, ganska många en stund senare och medan de sista stannar länge. Genom att mäta hur många som är kvar vid olika tider kan en medeltid beräknas, den tid som atomen förväntas vara kvar innan den åker in till en annan bana. Detta har vi kunnat mäta genom att låta atomerna cirkulera i en lagringsring med nästan vakuum. Det låga trycket minimerar kollisioners inverkan. De exciterade tillstånd i atomerna som vi har mätt är långlivade och elektronerna stannar väldigt länge innan de hoppar in. Länge, på en atomär skala, är några sekunder jämfört med miljarddels sekunder för normala tillstånd. Antalet atomer mäts genom att lysa på atomerna med en laser med en noga inställd våglängd. Endast de atomer som befinner sig i det tillståndet som mäts kommer då att detekteras. Emissionslinjer från de nivåer i järn och titan vi har mätt observeras i stjärnan Eta Carinae och dess omgivande gas, och de mätta livstiderna används i diagnostiken av plasmorna.

Vi har undersökt ljuset från den stora stjärnan Eta Carinae med Hubble-teleskopet (HST). Eta är en av de tyngsta och ljusstarkast stjärnorna i Vintergatan, med en massa på 130 solmassor och en luminositet flera miljoner gånger större. En av de stora fördelarna att observera från rymden, jämfört med markbaserade teleskop är att man även kan analysera ultraviolett och infrarött ljus som annars till stor del absorberas i jordens atmosfär. En annan är att man kan särskilja ljuset från platser som ligger nära varandra, relativt sett. Vi har speciellt undersökt ljuset från gasbubblor som ligger några ljusdagar från stjärnan. Eftersom avståndet till Eta Carinae är 7500 ljusår blir vinkeln mellan stjärnan och gasbubblorna ungefär en bågsekund, vilket är en 3600-dels grad. Det motsvarar att man från Lund kan titta på en buss i Stockholm och särskilja ljuset från de två olika strålkastarna. För varje strålkastare kan man dessutom noggrant separera färgerna hos ljuset, vilket t.ex. innebär att skilja på mer än 1000 olika nyanser i det röda ljuset.

Spektralanalysen, dvs tolkningen av de olika färger och våglängder som atomerna skickar ut, av de olika delarna av gasmolnen som vi har undersökt skall i förlängningen leda till en bättre förståelse för hur Vintergatans tyngsta stjärnor utvecklas. Dessutom har vi, med gasmolnen i Eta Carinae som hjälp, kunnat ta reda på hur atomer uppför sig under onormala betingelser. Den miljö som finns i dessa tunna gasmoln gör att vi kan mäta vissa egenskaper hos atomer som inte kan göras i laboratorier på jorden. Denna avhandling visar hur växelverkan mellan astrofysik och atomfysik inte bara ger fundamental kunskap om de stora stjärnorna i universum utan även om de små atomerna, var de än befinner sig.

References

Abrahamsson, K., Andler, G., Bagge, L., et al. 1993, Nuclear Instruments and Methods in Physics Research B, 79, 269

Andrä, H. J., Gaupp, A., & Wittmann, W. 1973, Phys. Rev. Letter, 31, 501

Bowen, I. S. 1928, ApJ, 67, 1

—. 1934, PASP, 46, 146

—. 1935, ApJ, 81, 1

—. 1947, PASP, 59, 196

Brown, A., Ferraz, M., & Jordan, C. 1981, in The Universe at Ultraviolet Wavelengths: The First Two Years of International Ultraviolet Explorer, 297–302

Brown, A. & Jordan, C. 1980, MNRAS, 191, 37P

Brown, A., Jordan, C., & Wilson, R. 1979, in The first year of IUE, ed. A. Willis, 232

Carpenter, K. G., Pesce, J. E., Stencel, R. E., et al. 1988, ApJS, 68, 345

Corcoran, M. 2003, http://lheawww.gsfc.nasa.gov/

Cowan, R. 1981, The Theory of Atomic Structure and Spectra (University of California Press, Berkeley, California)

Cowley, C. 1970, The Theory of Stellar Spectra (New York, Gordon and Breach)

Damineli, A. 1996, ApJL, 460, L49

Davidson, K. & Humphreys, R. M. 1997, ARA&A, 35, 1

Davidson, K., Ishibashi, K., Gull, T. R., & Humphreys, R. M. 1999, in Eta Carinae at the Millennium, ASP Conf. Ser. 179. Edited by J.A. Morse, R.M. Humphreys, and A. Damineli., 227

Edlén, B. 1941, Populär Astronomisk Tidskrift, hft. 1 & 2, 55

—. 1943, Zeitschrift fur Astrophysik, 22, 30

Ellmann, A. 2003, PhD thesis, Stockhom University

Garstang, R. 1962, in Atomic and Molecular Processes, ed. D. Bates (Academic Press, New York), 1

Garstang, R. H. 1962, MNRAS, 124, 321

Grotrian, W. 1939, Die Naturwissenschaften, 27, 214

Gull, T. & Ishibashi, K. 2001, in Eta Carinae and Other Mysterious Stars: The Hidden Opportunities of Emission Spectroscopy, ASP Conf. Ser. 242. Edited by T.R. Gull, S. Johannson, and K. Davidson. San Francisco: Astronomical Society of the Pacific, 59

Gull, T. R., Ishibashi, K., Davidson, K., & The Cycle 7 STIS Go Team. 1999, in Eta Carinae at the Millennium, ASP Conf. Ser. 179. Edited by J.A. Morse, R.M. Humphreys, and A. Damineli., 144

Haisch, B. M., Linsky, J. L., Weinstein, A., & Shine, R. A. 1977, ApJ, 214, 785

Hamann, F., Depoy, D. L., Johansson, S., & Elias, J. 1994, ApJ, 422, 626

Hartman, H. & Johansson, S. 2000, A&A, 359, 627

Hearnshaw, J. 1986, The analysis of starlight (Cambridge University Press, Cambridge)

Humphreys, R. M. & Davidson, K. 1994, PASP, 106, 1025

Humphreys, R. M., Davidson, K., & Smith, N. 2002, in ASP Conf. Ser. 279: Exotic Stars as Challenges to Evolution, 79–94

Ishibashi, K., Gull, T. R., Davidson, K., et al. 2003, AJ, 125, 3222

Johansson, S. 1983, MNRAS, 205, 71P

—. 1988, ApJL, 327, L85

Johansson, S. & Carpenter, K. G. 1988, in A Decade of UV Astronomy with the IUE Satellite, Volume 1, 361–363

Johansson, S., Derkatch, A., Donnelly, M., et al. 2002, Physica Scripta, T100, 71

Johansson, S. & Hamann, F. 1993, Physica Scripta, T47, 157

Johansson, S. & Jordan, C. 1984, MNRAS, 210, 239

Johansson, S. & Letokhov, V. S. 2003, Physical Review Letters, 90, 11101

Johansson, S., Wallerstein, G., Gilroy, K. K., & Joueizadeh, A. 1995, A&A, 300, 521

Johansson, S., Zethson, T., Hartman, H., et al. 2000, A&A, 361, 977

Johansson, S., Zethson, T., Hartman, H., & Letokhov, V. 2001, in Eta Carinae and Other Mysterious Stars: The Hidden Opportunities of Emission Spectroscopy, ASP Conf. Ser. 242. Edited by T.R. Gull, S. Johannson, and K. Davidson. San Francisco: Astronomical Society of the Pacific, 297

Jordan, C. & Harper, G. M. 1998, in ASP Conf. Ser. 154: Cool Stars, Stellar Systems, and the Sun, Vol. 10, 1277

Kastner, S. & Bhatia, A. 1986, Comments At. Mol. Phys., 18, 39

Kimble, R. A., Woodgate, B. E., Bowers, C. W., et al. 1998, ApJL, 492, L83

Leitherer, C. e. a. 2001, STIS Instrument Handbook, Version 5.1, (Baltimore: STScI)

Lidberg, J., Al-Khalili, A., Norlin, L.-O., et al. 1999, Nuclear Instruments and Methods in Physics Research B, 152, 157

Mannervik, S., Lidberg, J., Norlin, L. O., & Royen, P. 1997, Phys. Rev. A, 56, 1075

McMurry, A. D., Jordan, C., & Carpenter, K. G. 1999, MNRAS, 302, 48

Merrill, P. W. 1928, ApJ, 67, 391

Osterbrock, D. 1989, Astrophysics of Gaseous Nebulae and Active Galactic Nuclei (University Science Books, California)

Pauli, W. 1955, in Lunds Univ. Årsskrift avd 2:Proceedings of the Rydberg Centennial Conference on Atomic Spectroscopy, Vol. 50, 22

Quinet, P., Le Dourneuf, M., & Zeippen, C. J. 1996, A&AS, 120, 361

Redfors, A. & Johansson, S. G. 2000, A&A, 364, 646

Roberts, M., Taylor, P., Barwood, G. P., et al. 1997, Physical Review Letters, 78, 1876

Russell, H., Dugan, S., & Stewart, J. 1927, Astronomy, vol. II (Ginn and Company)

Rydberg, J. 1913, in Lunds Univ. Årsskrift, Vol. 9

Schmid, H. M. 1989, A&A, 211, L31

Shortley, G. H. 1940, Physical Review, 57, 225

Sikström, C. M., Nilsson, H., Litzen, U., Blom, A., & Lundberg, H. 2002, Journal of Quantitative Spectroscopy and Radiative Transfer, 74, 355

Smith, N., Morse, J., & Gull, T.R., et al. 2004, submitted to ApJ

Sobelman, I. 1979, Atomic spectra and radiative transitions (Springer Verlag)

Thackeray, A. D. 1937, ApJ, 86, 499

Thorne, A., Litzén, U., & Johansson, S. 1999, Spectrophysics: principles and applications (Springer Verlag)

Träbert, E., Calamai, A. G., Gwinner, G., et al. 2003, Journal of Physics B: Atomic, Molecular and Optical Physics, 36, 1129

Verner, E., Bruhweiler, F., Verner, D., Johansson, S., & Gull, T. 2003, ApJL, 592, L59

Viotti, R., Rossi, L., Cassatella, A., Altamore, A., & Baratta, G. B. 1989, ApJS, 71, 983

Wahlgren, G. M. & Carpenter, K. G. 1990, in ASP Conf. Ser. 9: Cool Stars, Stellar Systems, and the Sun. Edited by G. Wallerstein (Astronomical Society of the Pacific, San Francisco), 67

Weigelt, G. & Ebersberger, J. 1986, A&A, 163, L5

Woodgate, B. E., Kimble, R. A., Bowers, C. W., et al. 1998, PASP, 110, 1183

Zethson, T. 2001, PhD thesis, Lund University

Zethson, T., Hartman, H., Johansson, S., et al. 2001, in Eta Carinae and Other Mysterious Stars: The Hidden Opportunities of Emission Spectroscopy, ASP Conf. Ser. 242. Edited by T.R. Gull, S. Johannson, and K. Davidson. San Francisco: Astronomical Society of the Pacific, 97

Zethson, T., Johansson, S., Davidson, K., et al. 1999, A&A, 344, 211

Acknowledgements

I am grateful to all the people who helped me out with this work, and would like to thank some of them in particular.

Professor Sveneric Johansson, my supervisor, has provided superior guidance in the field of atomic spectroscopy and astrophysics since the first day of the Atomic Physics course, some 2506 (or maybe 2508) days ago. Your knowledge and never ending enthusiasm for this highly exciting and stimulating field is encouraging. Your inspiration and ingenious ideas have been the basis for my thesis.

The people at the Atomic Spectroscopy and Atomic Astrophysics groups have provided an excellent breeding ground by inspiring and professional science to accompany a good social atmosphere. Professor Ulf Litzén being the encyclopedia of spectroscopy, and Docent Glenn Wahlgren the astronomical dito are thanked for enthusiastically sharing their knowledge, and Professor Indrek Martinsson, Docent Jan-Olof Ekberg, Docent Sven Huldt and Mrs Sonja Mickelsson for making Atomic Spectroscopy a good home.

Present and former PhD and Master students within the group have created a unique fellowship and have thrown many good parties. I appreciate the trips to München and USA with Torgil, and a pleasant collaboration on the 'spectacular spectra from space'. Sharing offices with Hans, and for a while Krister, was pleasant although I never understood their fascination for English football.

The merge with the groups at Lund Observatory was fruitful and I made many new acquaintances.

I would like to express my appreciation for the warm hospitality from the group of Professor Sven Mannervik - LON, Peder, Danijela, Anna and the Peters - at Stockholm University during the many visits to CRYRING. You made the long night shifts memorable and introduced me in an instructive way to accelerator-based atomic physics. Docent Hans Lundberg, Lund Institute of Technology, made the travels to Stockholm fun and you shared your great knowledge in atomic physics in general and lifetime measurements in

particular. The CRYRING operators are acknowledged for providing excellent laboratory conditions.

For my enjoyable visits to NASA/GSFC I express my gratitude to Dr. Ted Gull for being an excellent host and collaborator. Your never ending enthusiasm for Eta Carinae and the will to extract every photon from each HST cycle is impressive and encouraging. Your and Connies cordial hospitality is greatly appreciated. Bish Ishibashi , thanks for being a careful scientist and sharing your knowledge in a great way. I remember the dinners and beers.

Finally, thanks to my family. I appreciate your support and interest in my work, although Atomic Astrophysics isn't your backyard. Linda, your love and warm support is wonderful, living with you is a privilege. Hedda, you light up my days with a smile and give an extra flavour to life.